Supplementary Information

Spectroscopic metrics allow in-situ measurement of mean size and thickness of liquid-exfoliated few-layer graphene nanosheets

Claudia Backes,[1] Keith R. Paton,[1] Damien Hanlon,[1] Shengjun Yuan,[2] Mikhail I. Katsnelson,[2] James Houston,[1] Ronan J. Smith,[1] David McCloskey,[1] John F. Donegan,[1] Jonathan N. Coleman[1]

[1]*School of Physics, CRANN and AMBER, Trinity College Dublin, Dublin 2, Ireland*

[2]*Institute for Molecules and Materials, Radboud University of Nijmegen, Heijendaalseweg 135, 6525AJ Nijmegen, the Netherlands*

*colemaj@tcd.ie

Contents

1 Size selection

1.1 TEM characterization

Transmission electron microscopy was used to measure the average lateral size of the graphene nanosheets in the dispersions. Sample preparation and imaging conditions are described in the *Methods* section. Figure S1 shows typical images of nanosheets from each dispersion, and the full set of histograms for graphene produced from Asbury graphite. From the histograms, the arithmetic number mean was determined and denoted as <L>.

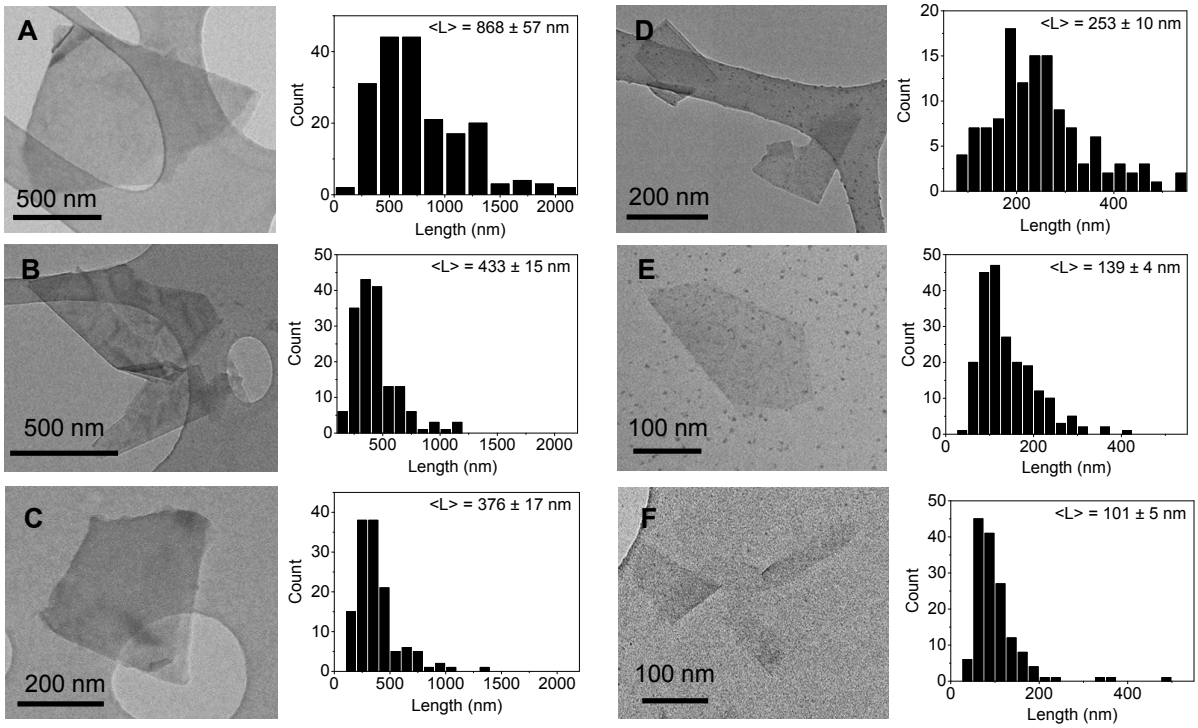

Figure S1: Representative TEM images of graphene produced from Asbury graphite, along with histograms of nanosheet length. Decreasing mean size A-F.

1.2 AFM characterization

Dispersions were characterized by AFM as described in the main text (see *Methods*), with the thickness, length and width measured. We note that once problems with deposition and converting the measured thickness to number of layers by using step height analysis[1-4] to account for residual surfactant and solvent, are overcome, we find AFM to give a more reliable estimate of the number of layers compared to TEM edge counting. This is because, in particular in this study, it was also necessary to count very small and thin flakes which are typically only found on the carbon support of the TEM grid and not over vacuum. In addition, the graphene produced from shear exfoliation is often folded making thickness determination by edge counting more tedious, as it is difficult to distinguish between a fold and different number of layers. It should also be noted that in general, TEM thickness determination by edge counting can be problematic, as nanosheets become thinner towards the edge. This means that multiple regions per nanosheet would need to be inspected to determine the mean thickness of one given nanosheet. In the case of AFM, this is much easier to do, as the measured thickness can easily be averaged over inhomogeneous nanosheets.

Figure S2 below shows typical AFM images from each fraction of samples exfoliated from Asbury graphite, along with histograms of nanosheet thickness (expressed as number of monolayers, N). Similarly, Figure S3 shows typical images and *N* histograms from samples exfoliated from Sigma Aldrich graphite. It is clear that dispersions produced from both graphite sources give size-selected samples with very similar distributions of nanosheet thickness. From the histograms, the arithmetic number mean was determined and denoted as <N>. We note that the thickness distributions become broader as the mean nanosheet thickness increases. However, a representative mean can be obtained when enough nanosheets are measured (>100) with standard errors < 0.5 even for dispersions containing the thickest nanosheets.

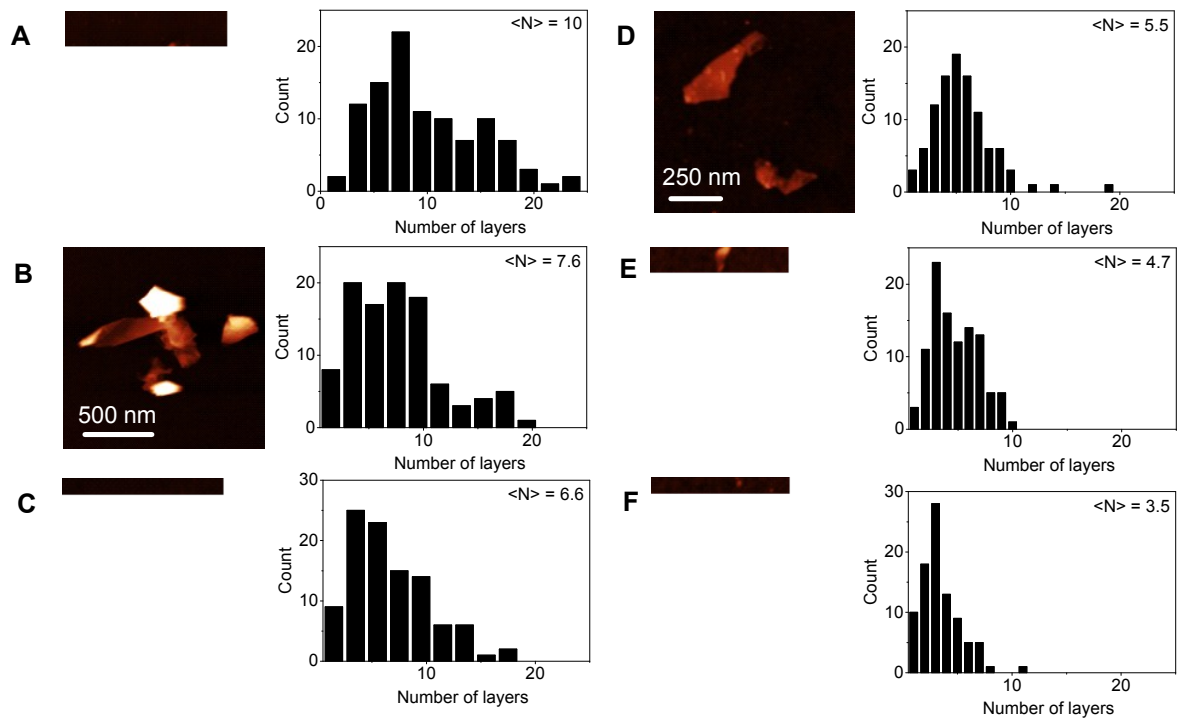

Figure S2: Representative AFM images and number of layer histograms of graphene produced from Asbury graphite. Decreasing sizes from A to F.

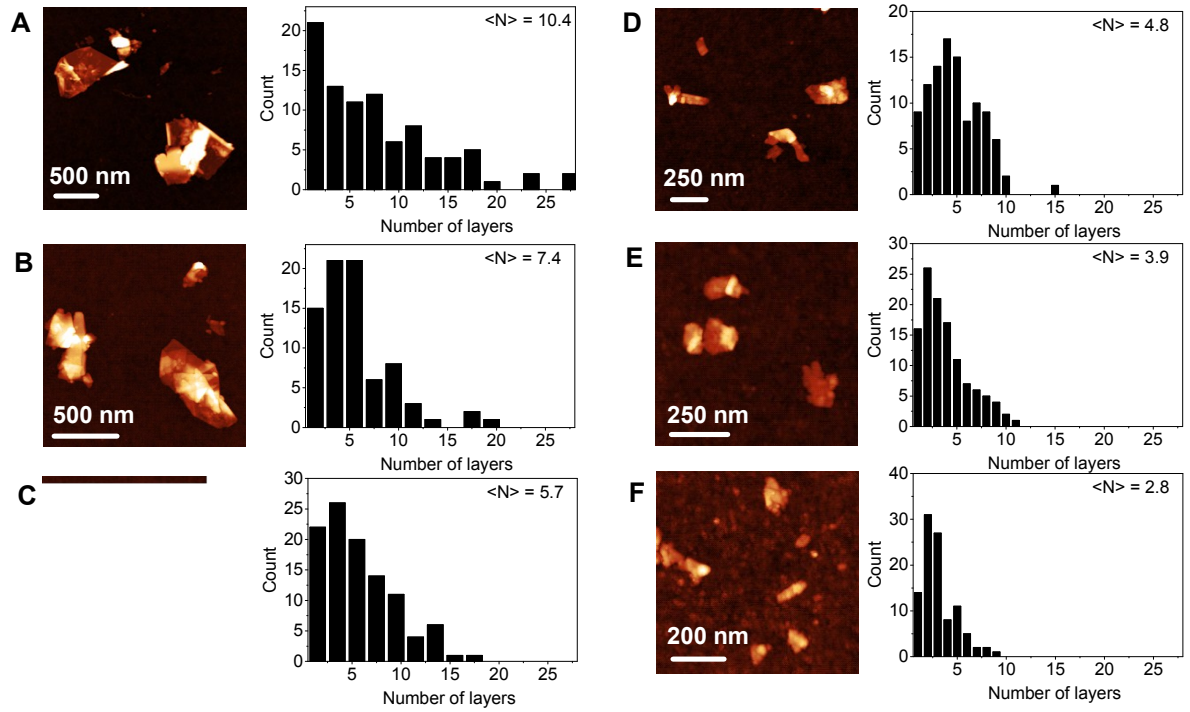

Figure S3: Representative AFM images and number of layer histograms of graphene produced from Sigma Aldrich graphite. Decreasing sizes from A to F.

We note that in the case of the Sigma Aldrich graphite samples, we sometimes find deposits that do not have well-defined edges such the ones in figure S4 top left. It is very likely that these objects are partially amorphous carbonaceous material. The thickness has been determined and values included in the counting to obtain the average value of <*N*>.

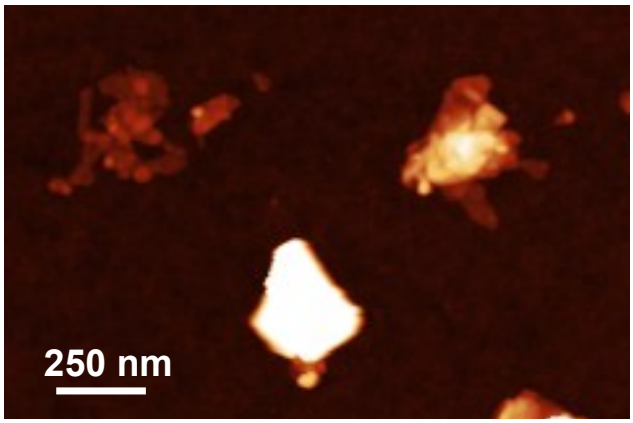

Figure S4: Example of an AFM image with deposits that do not have well-defined nanosheet edges found in the Sigma Aldrich graphite dispersions

Figure S5 shows a plot of number of monolayers *versus* basal plane area (expressed as length *x* width) for each nanosheet measured for Sigma Aldrich graphene. As was observed for Asbury graphene (see main text, figure 1H) there is only a weak correlation between the two parameters, with thinner nanosheets tending to be smaller.

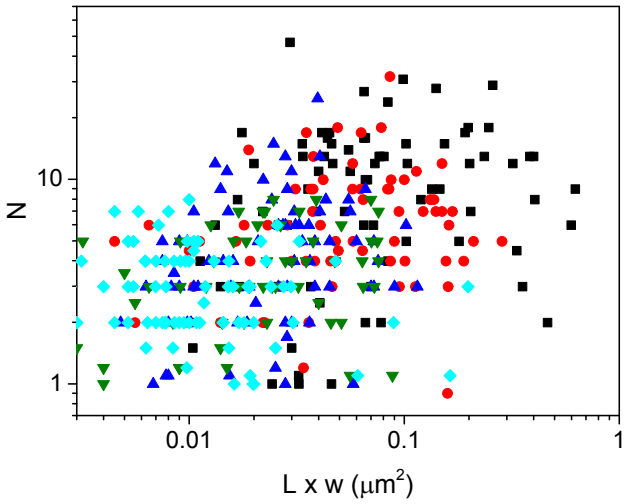

Figure S5: Number of layer, N, versus area (approximated as length x width) plot of the size-selected Sigma Aldrich graphene dispersions. Very similar to the dispersions produced from Asbury graphite, only a weak correlation between N and area is observed.

1.3 Stock dispersion

To establish the metrics, it is required that samples with various mean nanosheet sizes and thicknesses are produced. Therefore size selection was performed throughout this manuscript. However, for these metrics to be useful to optimize and monitor graphene production, the metrics will also need to be applicable to stock or stock-like (after mild centrifugation to remove unexfoliated material) dispersions. To test this, we have also analyzed a stock-like dispersion (supernatant after centrifugation at 1 krpm, 104 *g*) produced from shear-exfoliating Asbury graphite in aqueous SC. As shown by the representative AFM images in figure S6, the sample is highly polydisperse making AFM statistics more time-consuming. The length and thickness histograms (Fig. S6B and S6Cm respectively) confirm the broad distributions. Figure S6D shown an area *versus* thickness plot in analogy to the one in figure 1H, main manuscript. As expected, the plot basically represents roughly the sum of the individual data points of the size-selected samples.

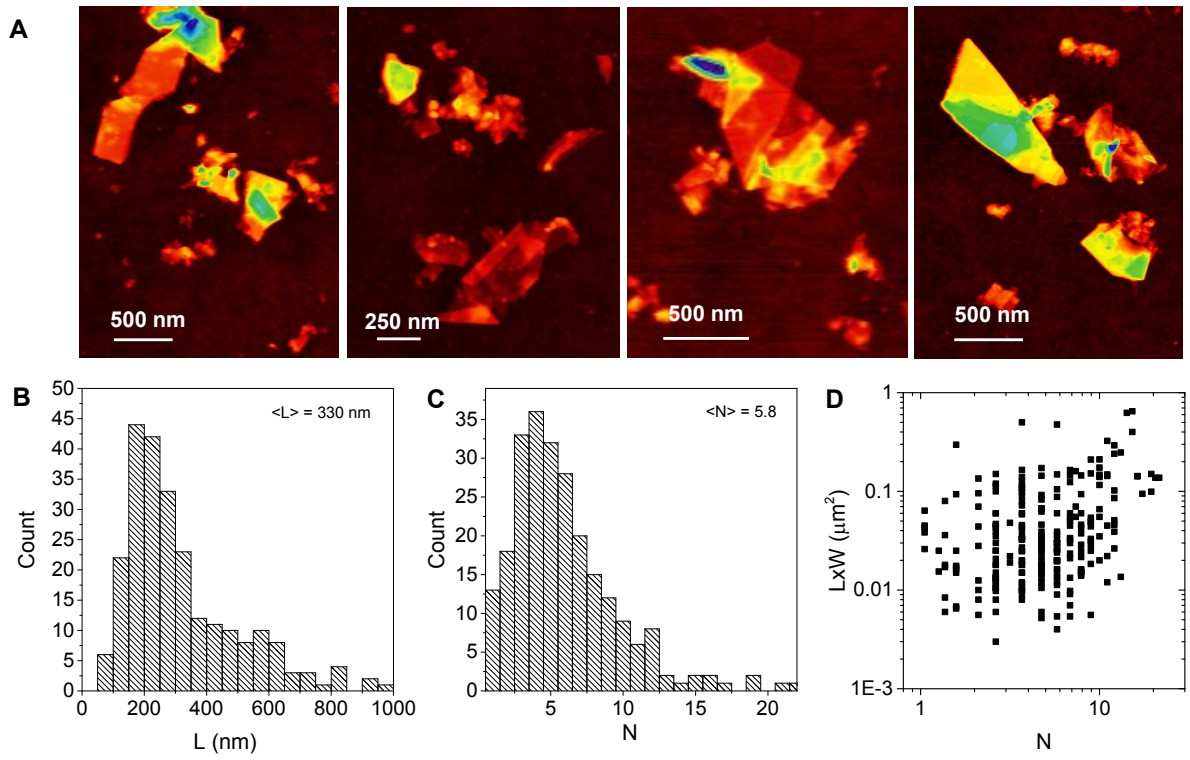

Figure S6:AFM characterization of a stock-like dispersion (supernatant after centrifugation at 1 krpm) of Asbury graphite shear-exfoliated in H_2O-SC. A) Representative images, B) Length histogram, C) Number of layer histogram, D) Plot of area (expressed as Lxw) versus layer number.

The spectroscopic data from the analysis of the stock-like dispersion is summarized in figure S7. Figure S7A shows the extinction, absorbance and scattering spectra and figure S7B the Raman spectra. Mean Raman spectra were acquired on a filtrered film (standard measurement) and compared to the result obtained from measuring the Raman spectrum on the liquid dispersion and a dried droplet, respectively. While the measurement on the filtered film and dried droplet (average of ~ 100 spectra) gives identical spectra, a different result is obtained in the case of the measurement in liquid. Significantly, the D-band is more intense and the 2D band also shows slight changes in shape. We attribute this mostly to orientation effects. In liquid, the nanosheets rotate randomly. However, in the dried state, they form randomly restacked networks with the nanosheets mostly lying flat on top of each other. Hence, the portion of nanosheets that are excited parallel to the edge is much smaller compared to the measurement in liquid. In addition, environmental effects may play a role. However, since the same spectrum is obtained from the dried droplet (not washed with surfactant adsorbed) and the filtered film (washed, surfactant partially removed), this is likely a minor effect in the case of our few-layer graphene. We note that the width of the G-band is similar in the spectrum of the liquid dispersion (23.1 cm^{-1}) compared to the filtered film (23.4 cm^{-1}) and dried droplet (23.6 cm^{-1}) suggesting that the length metric based on the width of the G-band is robust towards orientation effects.

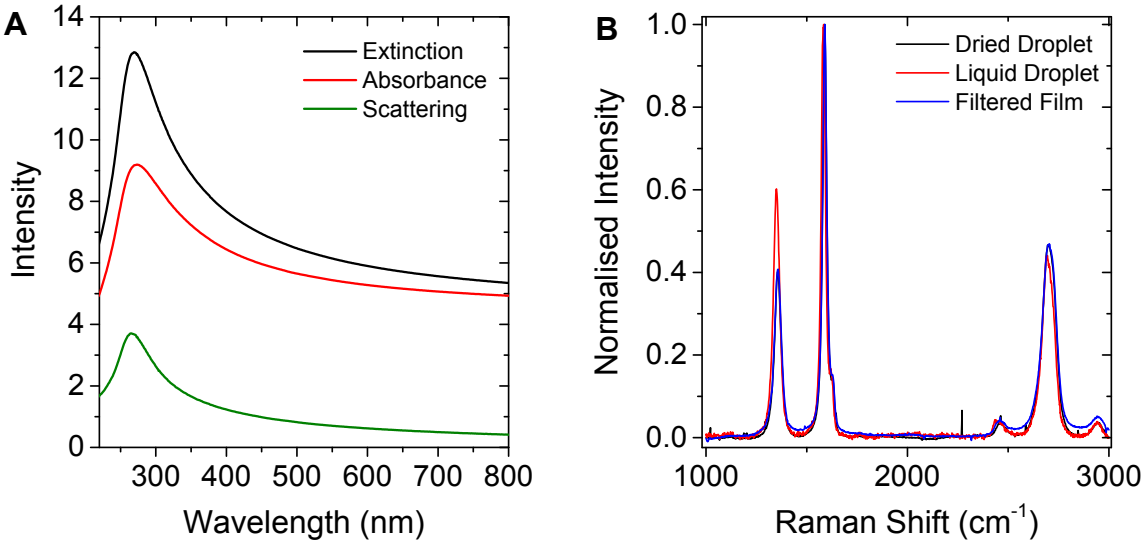

Figure S7:Spectroscopic characterization of the stock-like dispersion. A) Extinction, absorbance and scattering spectra. B) Raman spectra (excitation wavelength 532 nm) of a dried droplet, filtered film and the liquid dispersion as comparison. Filtered film and dried droplet gave identical results (average of 100 measurement acquired over an area of 20 x *20 µm²). The measurement in liquid yielded a slightly different Raman spectrum attributed mostly to orientation effects.*

1.4 Samples produceed by alternative exfoliation methods or in different media

To test the broader applicability of the metrics, it is important to analyze the impact of both exfoliation method and stabilizer in addition to the parent graphite source. Therefore, samples were also prepared by bath sonication and exfoliation in a kitchen blender in addition to the shear exfoliation in a rotor stator mixer used as standard production technique throughout this manuscript. Furthermore, the stabilizer was varied in some cases. Most samples were exfoliated in aqueous solutions of sodium cholate. However, tests were also performed using a kitchen soap (Fairy washing-up liquid) and *N*-methyl-2-pyrrolidone (NMP) as an example of a widely used solvent. These data points are included in figures 2 and 3 in the main manuscript, the spectroscopic and microscopic raw data is summarized in figures S8-S11. Unfortunately, the absorbance of NMP overlaps with the π-π^* transition of the graphene in the absorbance/extinction spectra. Therefore, this data is not accessible for the UV-Vis metric shown in the main manuscript. However, in figure S17, we show a plot of a different extinction intensity ratio (550 nm / 325 nm) *versus* nanosheet thickness with the data point from NMP included. All data falls on the same mastercurve suggesting that solvatochromic effects on the spectral profile are negligible in the case of few-layer graphene.

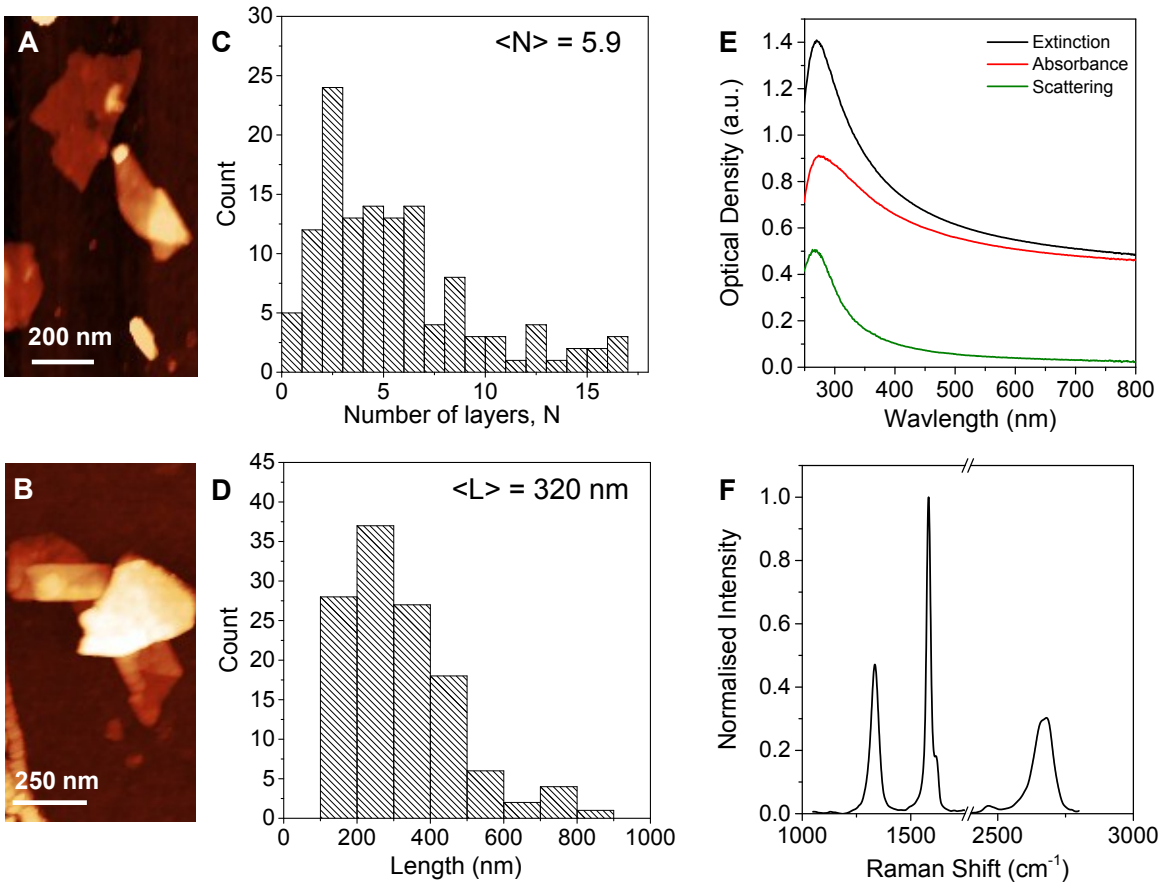

Figure S8: Microscopic and spectroscopic characterization of the Sigma Aldrich graphite exfoliated using a kitchen blender in aqueous fairy liquid. A, B) Representative AFM images, C) Number of layers histogram, D) Length histogram, E) Extinction, absorbance and scattering spectra, F) Raman spectrum of the filtered film (mean of 120 individual spectra).

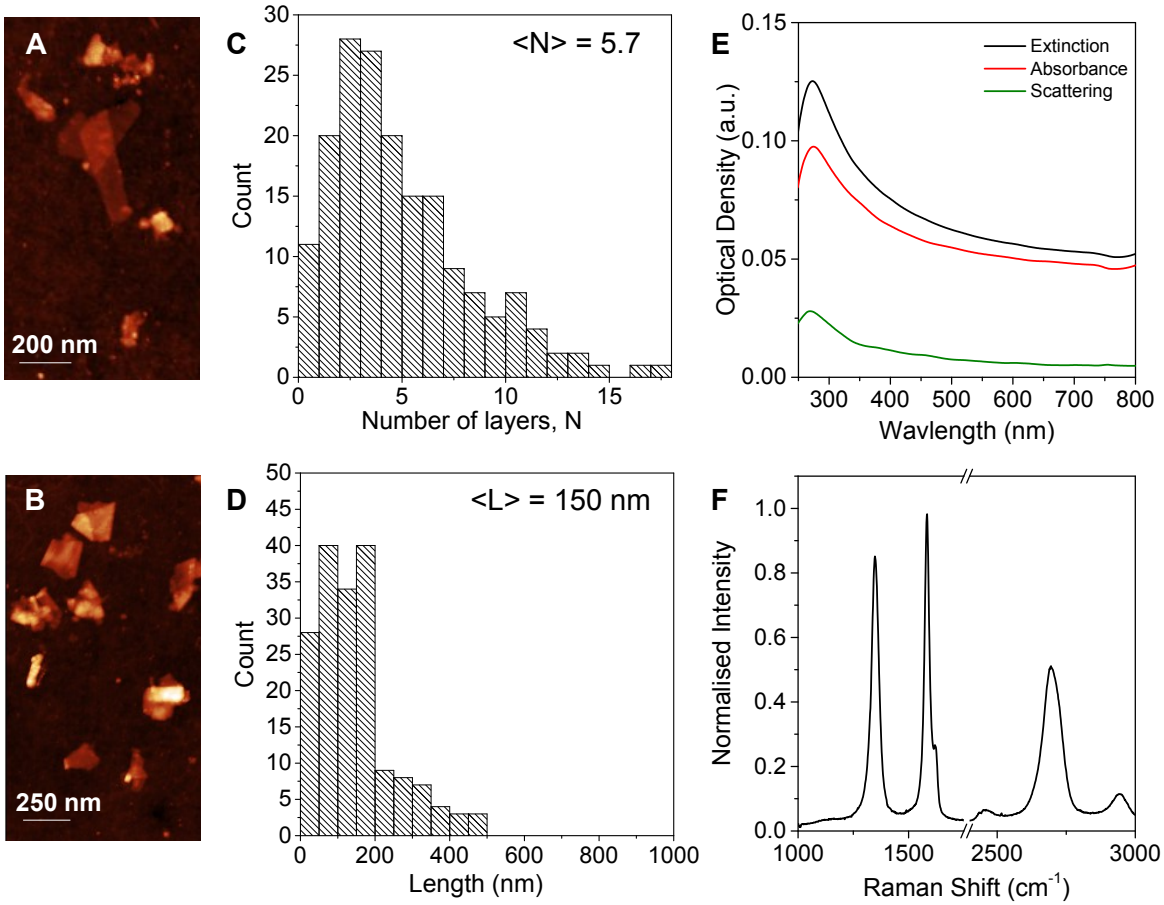

Figure S9: Microscopic and spectroscopic characterization of the Timrex graphite exfoliated using a sonic bath in aqueous SC. A, B) Representative AFM images, C) Number of layers histogram, D) Length histogram, E) Extinction, absorbance and scattering spectra, F) Raman spectrum of the filtered film (mean of 120 individual spectra).

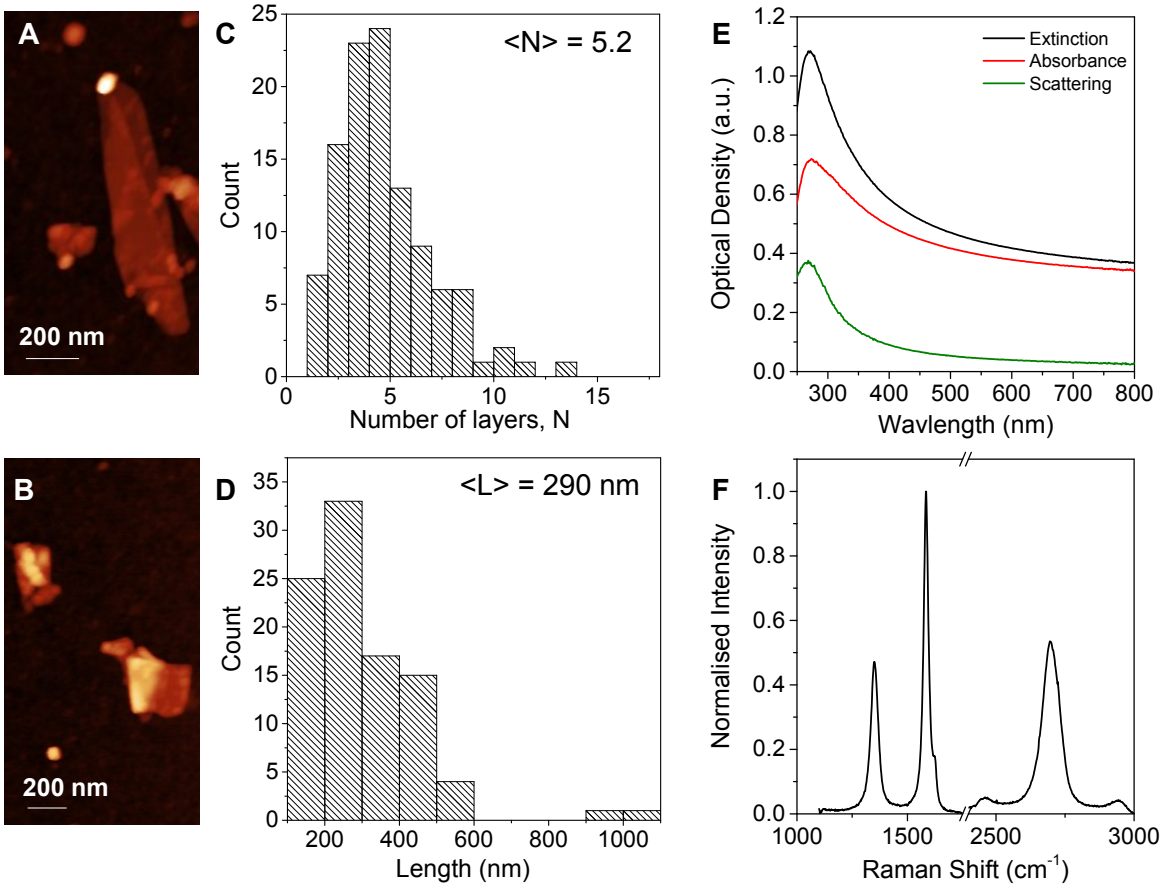

Figure S10: Microscopic and spectroscopic characterization of the Qingdao graphite exfoliated in a rotor-stator mixer in aqueous SC. A, B) Representative AFM images, C) Number of layers histogram, D) Length histogram, E) Extinction, absorbance and scattering spectra, F) Raman spectrum of the filtered film (mean of 120 individual spectra).

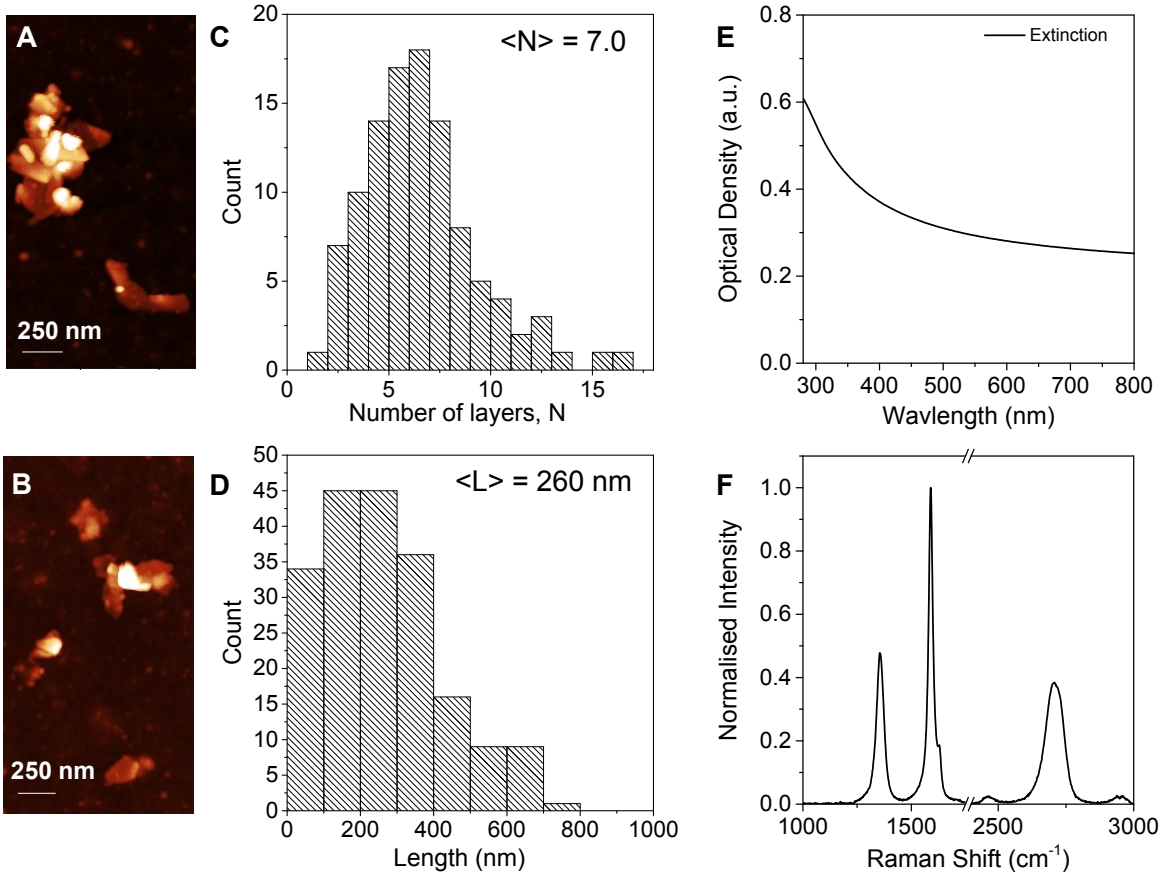

Figure S11: Microscopic and spectroscopic characterization of the Qingdao graphite exfoliated in a rotor-stator mixer in NMP. A, B) Representative AFM images, C) Number of layers histogram, D) Length histogram, E) Extinction spectrum, F) Raman spectrum of the filtered film (mean of 120 individual spectra). We note that deposition from high boiling points solvents leads to pronounced local aggregation and individual nanosheets are scarce. This renders the AFM thickness statistics extremely tedious and time-comsuming.

1.5 Mean length-thickness relation

Since we used centrifugation to obtain nanosheets of varying thickness and length distributions, we also tend to separate small and thin nanosheets from larger and thicker nanosheets. Hence, to some extend, <N> and <L> are linked after size-selection (even though the correlation is not as apparent on the flake by flake basis measurement as for other materials). To confirm that <N> and <L> can be determined independently from a spectrum, it is important to test samples with different <N>-<L> relationships. This is the case, when the exfoliation method (or stabilizer) is changed as shown in figure S12. For example, a typical sample of graphite shear-exfoliated (and size-selected) in H_2O-SC gives <L>=250 nm when <N>=5.5. For very similar thicknesses, bath sonication in H_2O-SC gives smaller nanosheets (<N>=5.7 and <L>=150nm), while exfoliation in fairy liquid in a kitchen blender gives larger ones (<N>=5.9 and <L>=320nm). We also note that the different parent graphite sources give a slightly different <N>-<L> relationship.

Importantly, with the exception of the Raman M_1 thickness metric, all data falls on the same mastercurve for both <N> and <L> metrics. This shows that <N> and <L> can indeed be independently determined from spectroscopy.

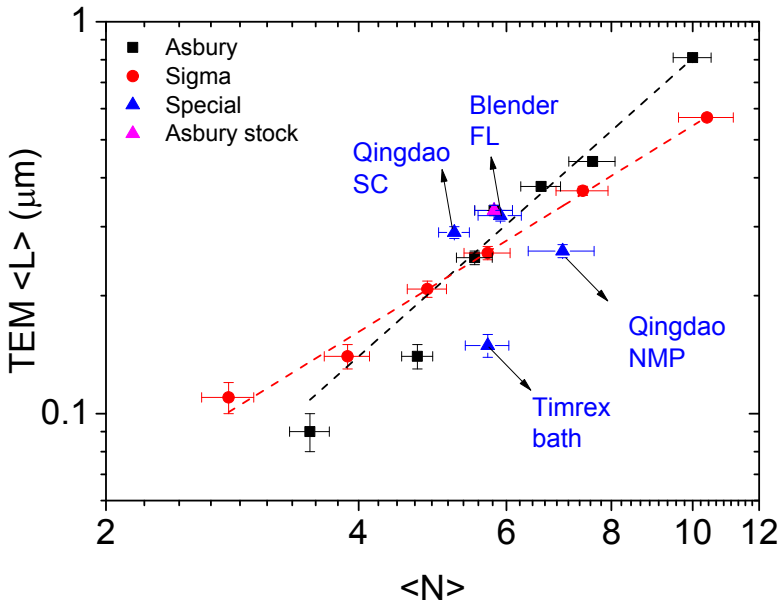

Figure S12: TEM mean length <L> plotted versus mean layer number determined from AFM. While size selection (set of black and red data points) results in a well defined relationship between <L> and <N>, this relationship is different across different types of samples.

2 Extinction/absorbance/scattering spectra

2.1 Simulated absorbance spectra with different stacking

It could be anticipated that different stacking of the graphene layers also has an impact to the absorbance spectroscopic profile in addition to layer number. To test whether this is the case, spectra were simulated with different stacking sequences. The data in the main manuscuscript (and figure S13A) was generated from ABA stacked graphene. As shown in figure S13B, a similar result is obtained in the case of ABC stacked graphene suggesting that the impact of stacking is negligible, especially when dealing with polydisperse samples as those produced from LPE. This is further confirmed when comparing experimental data from different exfoliation methods, as it can be assumed that these also result in a different restacking sequence in the obtained few-layer graphene dispersions. Notably, the thickness metric data from absorbance/extinction spectra falls on the same mastercurve in all cases.

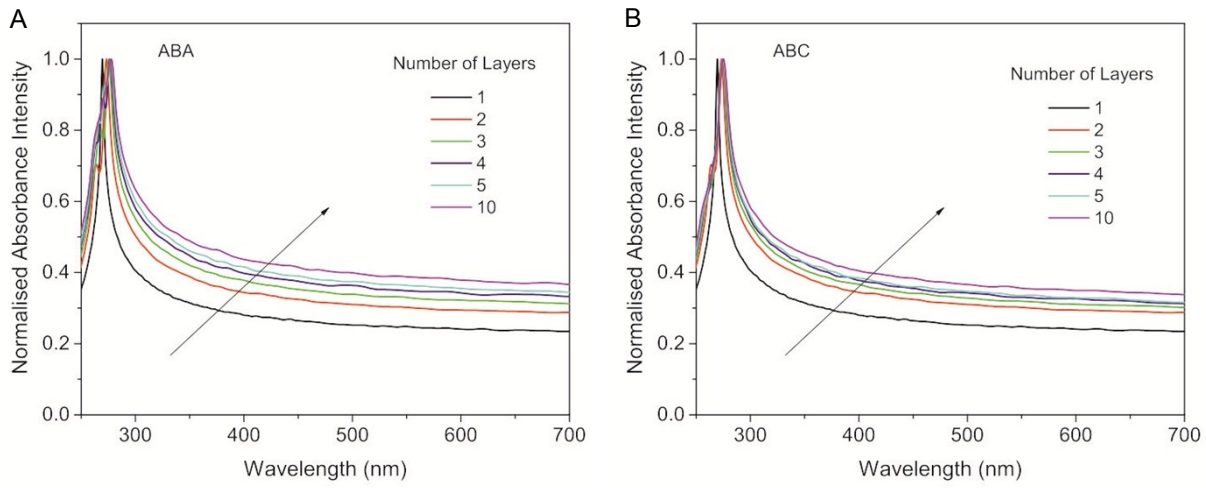

Figure S13: Simulated absorbance spectra normalized to the maximum for graphene of different thickness for A) ABA stacked sheets (main manuscript) and B) ABC stacked sheets.

2.2 Determination of residual surfactant by TGA

In order to determine extinction and absorbance coefficients reliably, it is necessary to measure the concentration of graphene in the dispersion by an alternative method. To obtain this measurement, we have filtered a measured volume of dispersion through membranes, and measured the mass of graphene deposited on the membrane. Despite rinsing with deionized water however, it is likely that some of the measured mass is residual surfactant on the graphene nanosheets. To quantify this, we have measured the weight loss by thermo-gravimeteric analysis, since the sodium cholate surfactant will oxidize at a lower temperature than the graphene. Figure S14 shows the weight loss curve, with two distinct weight-loss steps, one between 250 °C and 400 °C, attributed to the surfactant loss, and a second, larger weight-loss at ~650 °C due to the oxidation of the graphene. During the first weight-loss process, ~17.7% of the original weight is lost, indicating that the original measured mass of filtered graphene included 17.7 wt% surfactant. This is used to correct the graphene concentration and hence the extinction and absorbance coefficients.

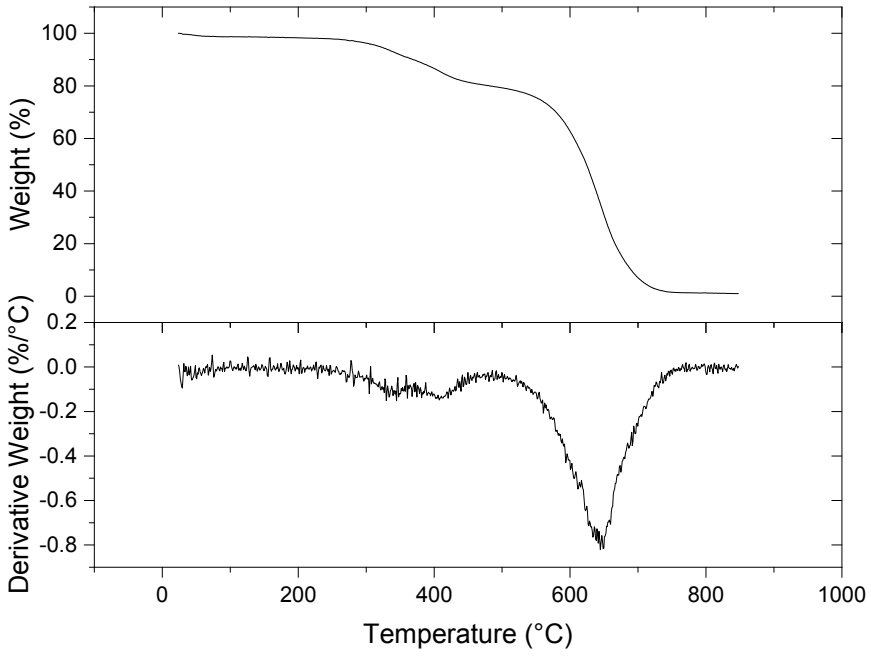

Figure S14: TGA weight-loss curve (top) and derivative weight-loss (bottom) from a filtered graphene dispersion. The weight-loss between ~250 °C and 400 °C is attributed to oxidation of residual surfactant and the main weight-loss peak centred at ~650 °C to the graphene oxidation.

2.3 Normalized spectra and spectra Sigma Aldrich graphite

Figure S15 shows the measured extinction and absorbance spectra for dispersions exfoliated from Asbury graphite. The spectra were normalized to the maximum intensity to allow changes in the spectral shape to be seen more clearly, in particular in comparison to the calculated absorbance spectra in the main manuscript. Extinction, absorbance and scattering spectra for dispersions exfoliated from Sigma Aldrich graphite are shown in figure S16. The trends seen for Asbury graphite are also seen in the Sigma Aldrich graphite based dispersions.

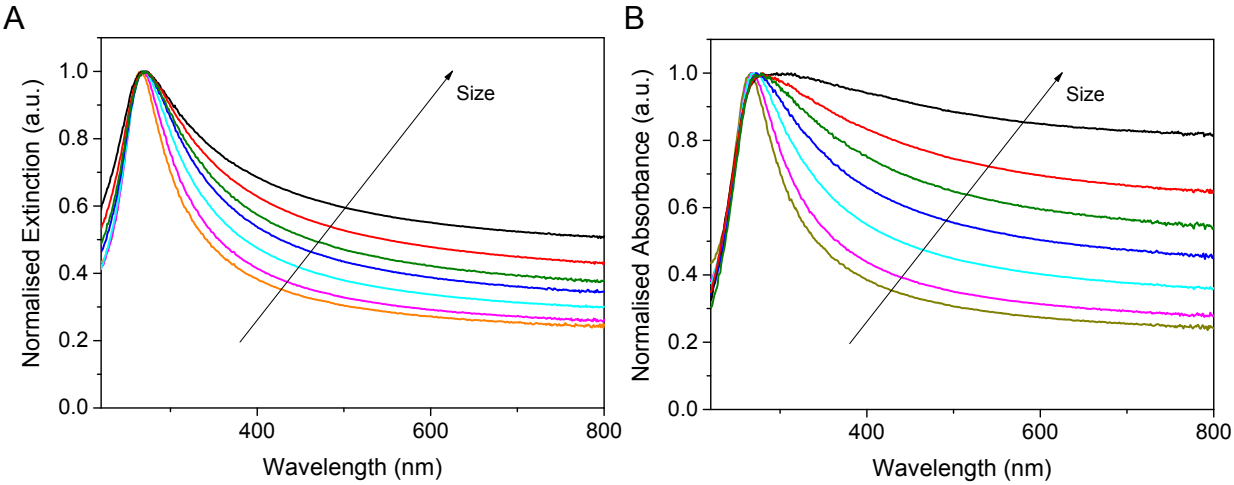

Figure S15: Normalized extinction (left) and absorbance (right) spectra for size-selected samples, produced from Asbury graphite.

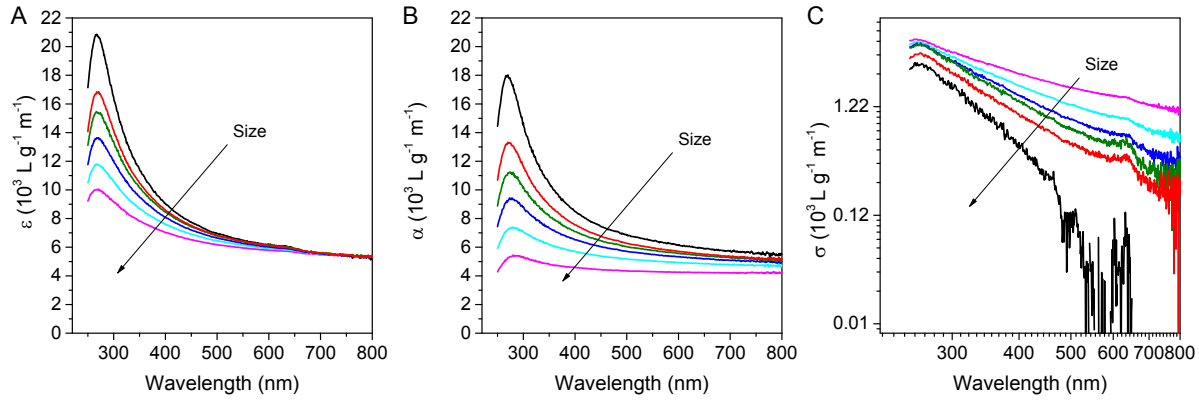

Figure S16: A) Extinction, B) absorbance and C) scattering coefficient spectra of the size-selected graphene dispersions produced from the Sigma Aldrich graphite.

2.4 N-metrics from extinction

Peak position

Both theoretical modelling and measurements on size-selected dispersions have shown that the position of the π-π* absorption peak can be used to quantify the average number of monolayers per nanosheet in a dispersion (see main text, figure 2A and 2E). However, this requires the removal of the scattering spectrum, and it would be more convenient if the same information could be extracted from the extinction spectrum. Figure S17 shows the position of the peak extracted from the extinction spectra of the samples. It is clear that for the smallest fractions, this also offers a useful metric, but cannot be used for mean nanosheet thicknesses above ~6.5 layers. The dashed line is an empirical fit to the data with small <N> and gives the following quantitative relation between the peak maximum from the extinction spectra and <N>.

$$\langle N \rangle = 0.81\ \lambda_{peak}\ (ext) + 213 \qquad (S1)$$

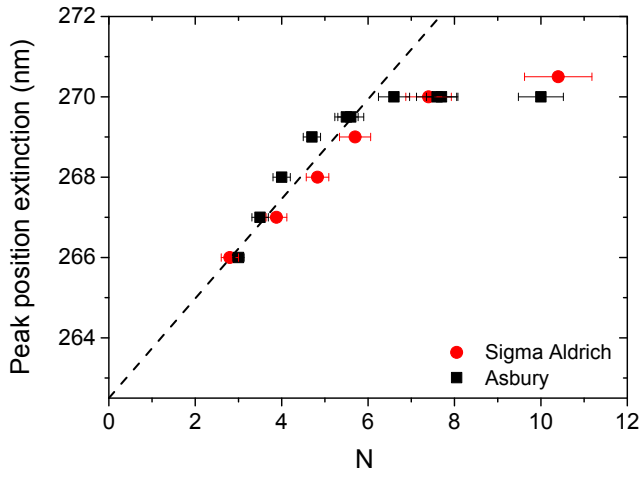

Figure S17: Position of π-π peak in intensity ratio as a function of average nanosheet thickness measured from extinction spectra. The dashed line is a fit to equation S1.*

Alternative peak intensity ratio for solvents

While the measurement of absorbance spectra shown and analyzed in the main manuscript was necessary to confirm that the spectral profile of LPE graphene changes as a function of layer number, extinction spectra are probably more practical because they can be

measured using standard lab equipment. As shown in the main manuscript, the peak intensity ratio at the plateau region and the maximum gives a good metric for the number of layers. Unfortunately, many commonly used solvents such as NMP absorb light at <300 nm masking the graphene π-π* transition. In figure S18 we therefore plot the extinction intensity ratio at 550 nm / 325 nm to establish a quantitative relationship (equ. S2) that can also be used in the case of solvents such as NMP.

$$\langle N \rangle = 35.7 \times \varepsilon_{550} / \varepsilon_{325} - 14.8 \qquad \text{(S2)}$$

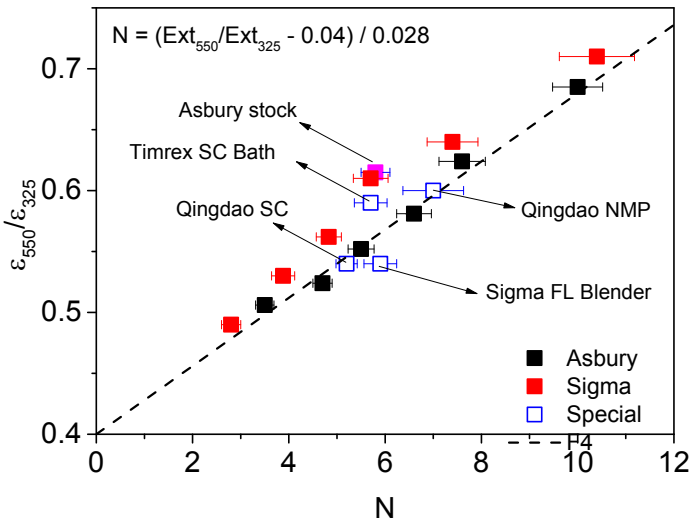

Figure S18: Extinction intensity ratio at 550 nm / 325 nm plotted as a function of mean number of layers of the LPE graphene. Data from varying exfoliation methods and stabilizer are included as indicated in the figure. Notably, the data from graphite exfoliated in NMP falls on the same curve suggesting solvatochromic effects to be negligible in the case of the few-layer graphene typically obtained in the process.

2.5 Scattering length metrics

Previous work has suggested that information about the lateral size of nanosheets is contained in the exponent of the scattering spectrum. For materials with negligible absorbance in the wavelength range of interest, and for wavelengths above a critical value, the scattering coefficient tends to vary with wavelength as a power law: $\sigma(\lambda) \propto \lambda^{-n}$. For small particles, n=4 as described by Rayleigh scattering while for larger particles, Mie scattering predominates resulting in a size-dependent n ($0<n<4$).[5]

For the graphene dispersions prepared in the present work, we indeed find the scattering exponent to be between 0 and 4 with some size-dependence indicated for larger nanosheets (Figure S19A). However, the data is very scattered and the relation between the scattering exponent and the lateral sizes is only poorly defined. We attribute this to the fact that graphene has a significant absorbance, such that the signal-to-noise ratio of the scattering spectra is very low. Therefore, the determination of the scattering exponent is not accurate and it cannot be used as reliable metric to determine L.

However, since the absorbance is essentially flat at high wavelengths (650-800 nm), a measure for the scattering exponent can be obtained from the extinction spectra. We note that this is technically not the scattering exponent, but the scattering exponent plus a constant value due to the absorbance background. We plot this exponent from the extinction spectra as a function of mean <L> of the graphene in Figure S19B and find a reasonably well-defined relation giving a potential metric to determine <L> from the extinction spectra according to equation S3. While this provides a better metric than attempting to determine the scattering exponent from the scattering spectra, it still breaks down for the dispersions with graphene of L<200 nm. Currently, it is not clear whether this is because the scattering spectrum is then dominated by Rayleigh scattering (where the scattering exponent should saturate at around 4).

$$< L >= \left(\frac{Ext.\ exp.}{2.466}\right)^{-3.05} \quad \text{(S3)}$$

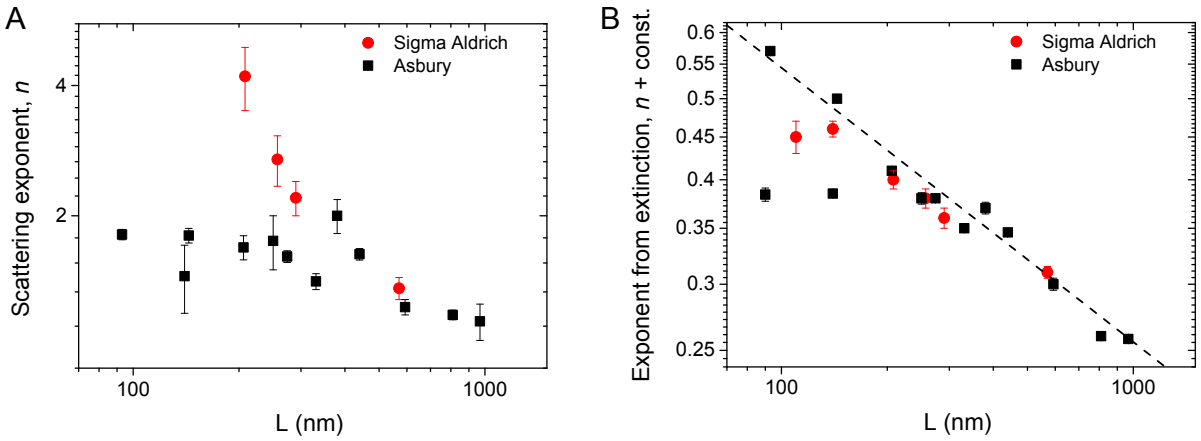

Figure S19 A) Scattering exponent (determined between 650-800 nm) determined from the scattering spectra as a function of mean lengths of the graphene nanosheets. B) The exponent determined from the extinction spectra (650-800 nm) plotted as a function of mean length. The dashed line is a fit to equation S2 and gives a reasonably good metric to determine L from the extinction spectra. N.B. The determination of the scattering coefficient from the scattering spectra is not possible in every case for L< 200 nm, as spectra are very noisy with average intensities close to zero.

2.6 Coefficients at different wavelengths

From the extinction coefficient spectra, it is very clear that the plateau region is ideal to determine the concentration of liquid-exfoliated graphene, as the extinction coefficient is largely size-independent in this region. This is clearly not the case for the absorbance and extinction coefficient at the peak in the spectrum as plotted in Figure S20A. In Figure S20B, we furthermore plot the coefficients at 660 nm because this wavelength has previously been frequently used to estimate the concentration of liquid-exfoliated graphene.[6, 7] Similarly to the data shown in the main manuscript, the coefficients are also widely size independent.

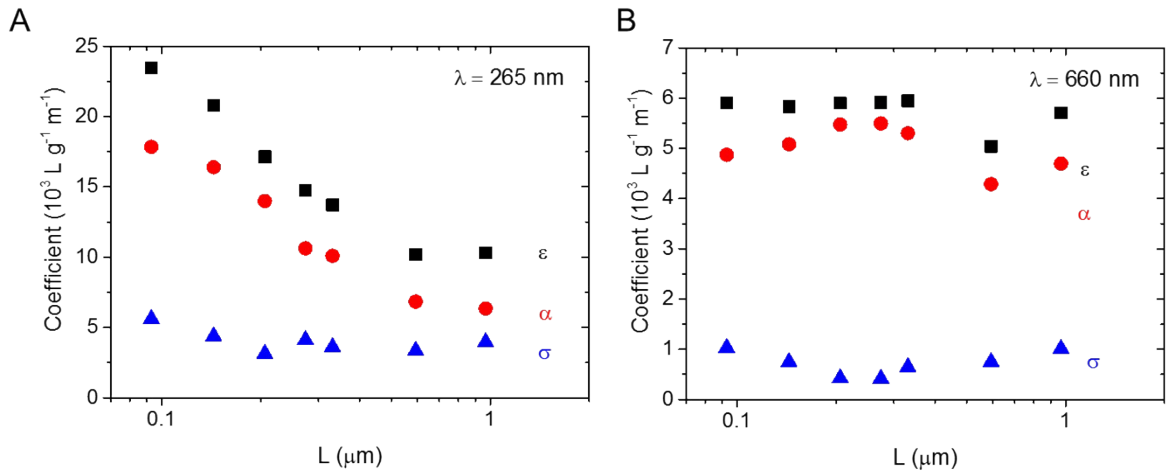

Figure S20: Extinction, absorbance and scattering coefficients plotted as a function of graphene lateral dimension expressed as mean length, L at A) the peak at ~ 265 nm and B) close to the plateau region at 660 nm.

3 Raman spectroscopy

3.1 Effect of laser power on metrics

In order to confirm the robustness of the metrics derived from Raman spectroscopy, we have tested the effect of measurement conditions. It is commonly known that high intensity laser irradiation can lead to damage to graphene samples, and changes in the spectrum due to local heating. To investigate how this affects the metrics we have derived, we have systematically varied the laser intensity incident on our sample. As shown in Figure S21 the most striking change is in total signal intensity as the laser power in increased. It is also worth noting that even at the highest power (10 mW) the spectrum has the typical appearance re-aggregated graphene nanosheets. However, as discernible from the normalized spectra in figure S21B, systematic spectral changes occur as the laser power is increased.

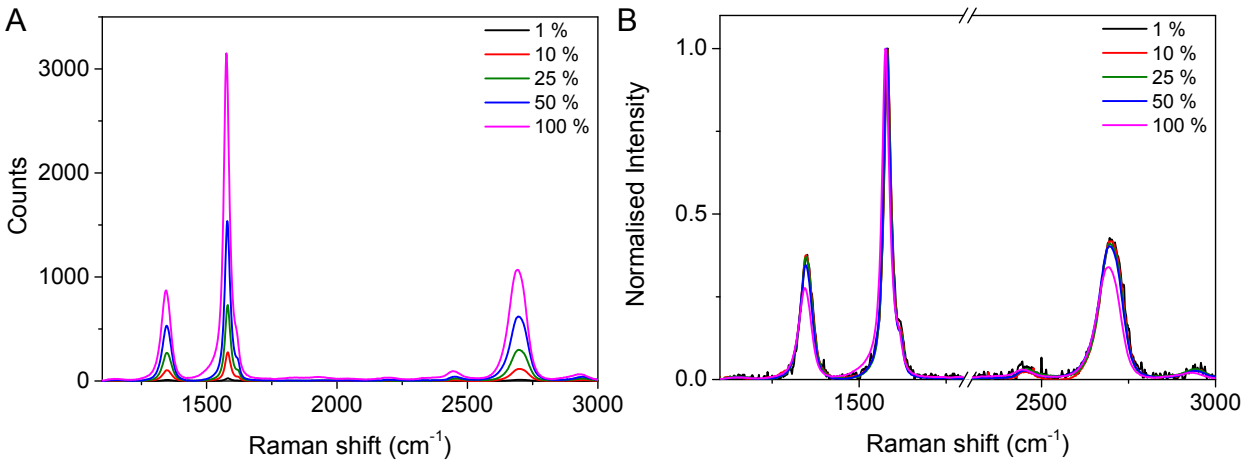

Figure S21: Raman spectra measured as a function of laser intensity. A) As-recorded spectra, B) spectra normalized to the G-band.

When plotting the I_D / I_G ratio as a function of laser power, it is clear that there is a threshold above which the ratio falls (Figure S22A). This would imply that the nanosheets in the sample being measured are larger than they actually are (290 nm at <25% compared to 320 nm at 100 %), and emphasizes the importance of using low laser intensity for reliable measurements especially when a quantification of size is targeted. In order to minimize measurement time and to reduce the impact of local heating, we have used 10 % of the laser intensity (1 mW) to establish the metrics described in the main manuscript.

We have also plotted the effect of laser intensity on the other metrics described in the main text, all of which show some variation. The G-band width (Figure S22B) shows a complicated behaviour, with the minimum width found for 25% laser power, the value of the threshold for I_D / I_G ratio. When using the metric equation (eq. 5 in the main manuscript), the deviation across laser intensities would relate to variations in <L> from 200 nm (at 100%) to 320 nm (at 25 %). These variations are significant so that care must be taken to use similar (low) laser powers when for the G-band width as quantitative metric.

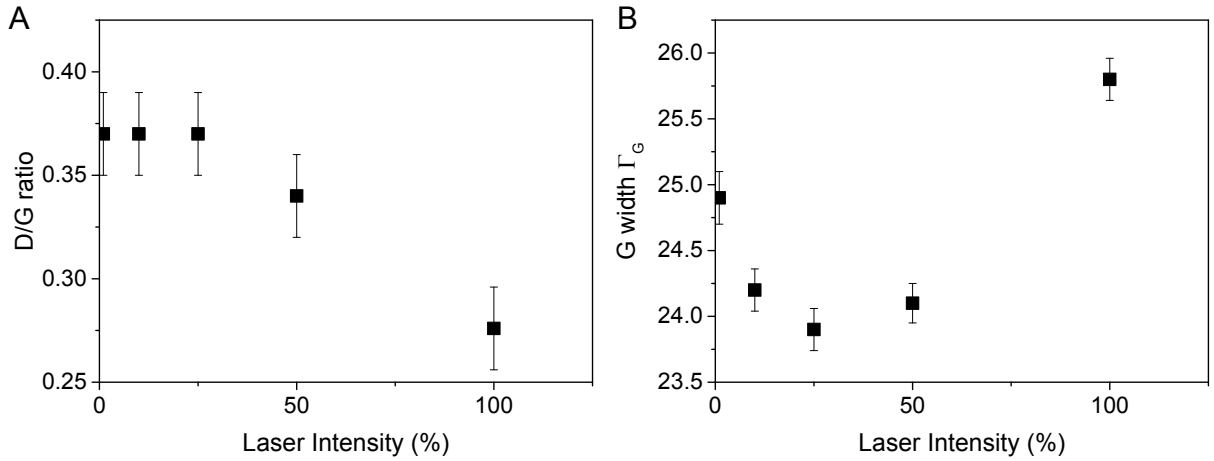

Figure S22: A) I_D / I_G (left) and Γ_G (right) plotted as a function of laser intensity. A clear threshold is seen at 25% (2.5 mW) below which the ratio is invariant with laser power. Above this threshold, the metric implies that the sample contains larger nanosheets. The empirical fits derived in the main text were obtained at 10% laser intensity. B) G-width Γ_G as a function of laser power showing a complex behavior with laser power.

The M_1 thickness metric also shows a threshold, this time at 50% (Figure S23A). Note however, that in this case, the value of the metric does change systematically below this threshold, although the changes are only small (within error) relating to variations of < 1 layer. At the highest laser power, the metric would suggest the nanosheets to be significantly thicker (12.5 opposed to 7.5 layers).

Figure S23B shows the variation in the thickness metric M_2 described in the main text as the laser power is changed. As for the I_D / I_G metric, there is a threshold below which there is no change in the value. In this case, this threshold is seen at 10% rather than 25%. At high laser

powers, the graphene nanosheets appear significantly thinner (3.8 layers in mean at 100% laser power compared to 5.5 at 10%) according to M_2.

Obviously, the M_1 thickness metric is more robust towards spectral shifts compared to M_2 and also towards measurement at different laser powers. However, it suffers from the serious drawback that we observed that M_1 is less reobust towards changes in the stabilizer (see main manuscript).

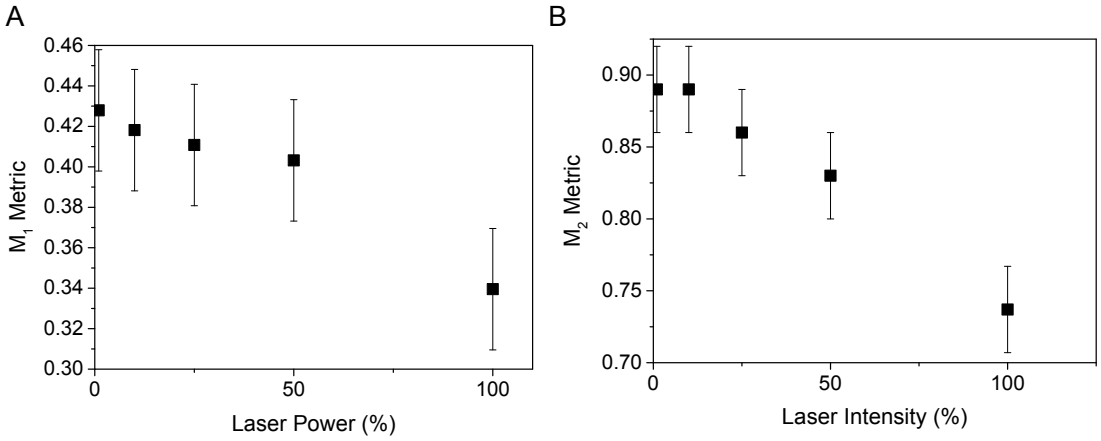

Figure S23: Effect of laser power on thickness metrics, A) M_1 and B) M_2.

3.2 Impact of the grating on metrics

Finally, the effect of the grating used in the spectrometer has been examined, by plotting the metrics using the 600 mm^{-1} and 1800 mm^{-1} gratings. The latter provides a higher spectral resolution (~0.5 cm^{-1} compared to ~1.5 cm^{-1} for the 600 mm^{-1}), but at the expense of lower signal intensity and slower scan times. Figure S24 shows the metrics described in the main text plotted against one another. Both I_D / I_G and G-width metrics are quite robust against measurement with high or low resolution gratings except for the smallest sizes, where measurement with the high resolution grating would underestimate the lateral size.

The metrics for thickness, based on the 2D band are largely invariant against a change in grating except M_1 where values are consistently larger when using the 1800 mm^{-1} grating. We note that for establishing the metrics, the 600 mm^{-1} grating was used.

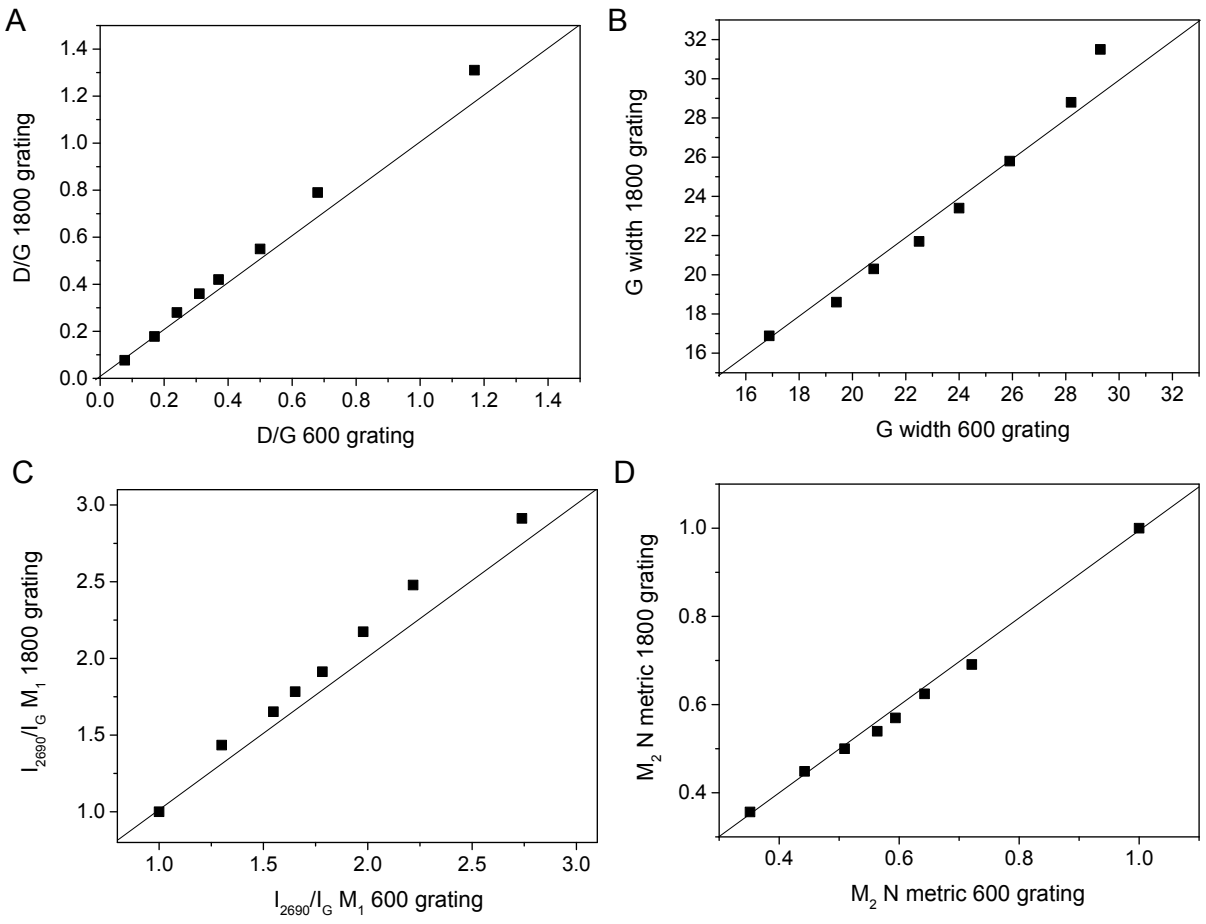

Figure S24: Effect of grating choice on values of metrics, confirming that they are all largely invariant with the grating used. The exception is the M_1 thickness metric, where there is clear deviation between overview and high resolution grating for the thinnest fractions.

3.3 Relationship between D/G ratio and nanosheet length

For an ensemble of graphene nanosheets, The D-band contains contributions associated with the edge defects and any point defects in the basal plane while the G-band intensity is just proportional to the number of "graphitic" carbon atoms seen by the laser. The ratio of intensities of the D- and G-bands can be written as

$$\frac{I_D}{I_G} = \frac{I_{D,\text{edge}}}{I_G} + \frac{I_{D,\text{point}}}{I_G} \tag{S3}$$

We can express the three quantities on the right hand side of this equation as follows:

$$I_{D,\text{edge}} = C_{D,\text{edge}} \frac{N_{D,\text{edge}}}{L} \sum_{Flakes} L_{\text{edge}} \tag{S4}$$

Where $C_{D,\text{edge}}$ is a constant which relates the measured intensity to the number of edge defects seen by the laser (signal intensity per defect), $N_{D,\text{edge}} / L$ is the number of edge defects per unit length of nanosheet edge and $\sum_{Flakes} L_{\text{edge}}$ is the sum of the lengths of all flakes seen by the beam.

$$I_{D,\text{point}} = C_{D,\text{point}} \frac{N_{D,\text{point}}}{A} \sum_{Flakes} A_{\text{basal}} \tag{S5}$$

Where $C_{D,\text{point}}$ is a constant which relates the measured intensity to the number of basal plane point defects seen by the laser, $N_{D,\text{point}} / A$ is the number of point defects per unit area of basal plane and $\sum_{Flakes} A_{\text{basal}}$ is the sum of the basal plane areas of all flakes seen by the beam.

$$I_G = C_G \frac{N_{C-atom}}{A} \sum_{Flakes} A_{\text{basal}} \tag{S6}$$

Where C_G is a constant which relates the measured intensity to the number of basal plane C-atoms seen by the laser, N_{C-atom} / A is the number of C-atoms per unit area of basal plane and $\sum_{Flakes} A_{\text{basal}}$ is the sum of the basal plane areas of all flakes seen by the beam. N.B The "C" constants incorporate (and average) factors such as scattering cross-section of the defect, any polarisation or instrumentation effects etc.

Then the D/G ratio is given by

$$\frac{I_D}{I_G}=\frac{I_{D,\text{edge}}}{I_G}+\frac{I_{D,\text{point}}}{I_G}=\frac{C_{D,\text{edge}}\dfrac{N_{D,\text{edge}}}{L}\displaystyle\sum_{Flakes}L_{\text{edge}}}{C_G\dfrac{N_{C-atom}}{A}\displaystyle\sum_{Flakes}A_{\text{basal}}}+\frac{C_{D,\text{point}}\dfrac{N_{D,\text{point}}}{A}\displaystyle\sum_{Flakes}A_{\text{basal}}}{C_G\dfrac{N_{C-atom}}{A}\displaystyle\sum_{Flakes}A_{\text{basal}}} \tag{S7}$$

The second term on the righ hand side is identical to the D:G ratio of the parent graphite ($(I_D/I_G)_{G'ite}$), assuming the graphite flakes are large enough that the edge defect content is very small and can be neglected. In addition, the first term can be simplified by combining all constants into one constant k': $k'=C_{D,\text{edge}}(N_{D,\text{edge}}/L)/C_G(N_{C-atom}/A)$, giving:

$$\frac{I_D}{I_G}=\left(\frac{I_D}{I_G}\right)_{G'ite}+k'\frac{\displaystyle\sum_{Flakes}L_{\text{edge}}}{\displaystyle\sum_{Flakes}A_{\text{basal}}} \tag{S8}$$

We assume the laser beam probes *m* graphene flakes. In addition, for a given nanosheet the edge length is related to the nanosheet length (longest dimension, L) by $L_{\text{edge}}=SF_L\times L$ where SF_L is a shape factor specific to that nanosheet. Then

$$\sum_{Flakes}L_{\text{edge}}=\sum_{Flakes}SF_L\times L=m\langle SF_L\times L\rangle\approx m\langle SF_L\rangle\langle L\rangle \tag{S9}$$

Similarly, for a given nanosheet the basal plane area is related to the nanosheet length (longest dimension, L) by $A_{\text{basal}}=SF_A\times L^2$ where SF_A is a second shape factor specific to that nanosheet. Then

$$\sum_{Flakes}A_{\text{basal}}=\sum_{Flakes}SF_A\times L^2=m\langle SF_A\times L^2\rangle\approx m\langle SF_A\rangle\langle L\rangle^2 \tag{S10}$$

This means

$$\frac{I_D}{I_G}=\left(\frac{I_D}{I_G}\right)_{G'ite}+k'\frac{\displaystyle\sum_{Flakes}L_{\text{edge}}}{\displaystyle\sum_{Flakes}A_{\text{basal}}}\approx\left(\frac{I_D}{I_G}\right)_{G'ite}+k'\frac{m\langle SF_L\rangle\langle L\rangle}{m\langle SF_A\rangle\langle L\rangle^2} \tag{S11}$$

Rearranging and relabelling slightly, we get

$$\left(\frac{I_D}{I_G}\right)_{G'ene}-\left(\frac{I_D}{I_G}\right)_{G'ite}\approx k'\frac{\langle SF_L\rangle}{\langle SF_A\rangle}\frac{1}{\langle L\rangle}=\frac{k}{\langle L\rangle} \tag{S12}$$

We note that *k'* should be the same for graphenes (unless some edge passivation has occurred). However, $\langle SF_L \rangle / \langle SF_A \rangle$ depends on the distribution of flake shapes and so may vary somewhat for different production methods. This means that there is some scope for *k* to vary from the value measured in this paper.

3.4 Analysis of the $I_D/I_{D'}$ ratio to assess defect type

It has previously been shown by Eckmann *et al.* that different defects result in changes of the $I_D/I_{D'}$ intensity ratio.[8] For example, sp^3 defects show $I_D/I_{D'}$ intensity ratio of ~13, vacancy defects a ratio of ~7 and edge defects are quoted as ~3.5 . Hence, a plot of the I_D/I_G ratio as function of $I_{D'}/I_G$ can serve as indicator for the defect type. This is plotted in figure S25. The intensities were obtained from fitting the G-band and D' band region to two Lorentzians. We obtain an $I_D/I_{D'}$ intensity ratio of 4.9 which is inbetween the quoted values for vacancy and edge defects. A problem with this analysis is however that basal plane defects present also in the parent graphite (and therefore all exfoliated nanosheets) cannot be corrected for unlike the analysis of the I_D/I_G ratio as discussed in section 3.3. This does not imply that basal plane defects are introduced on exfoliation as extensively discussed in one or our previous reports, where we show that $I_D/I_{D'}$ as low as ~4.2 were observed when an even higher quality parent graphite was used.[2]

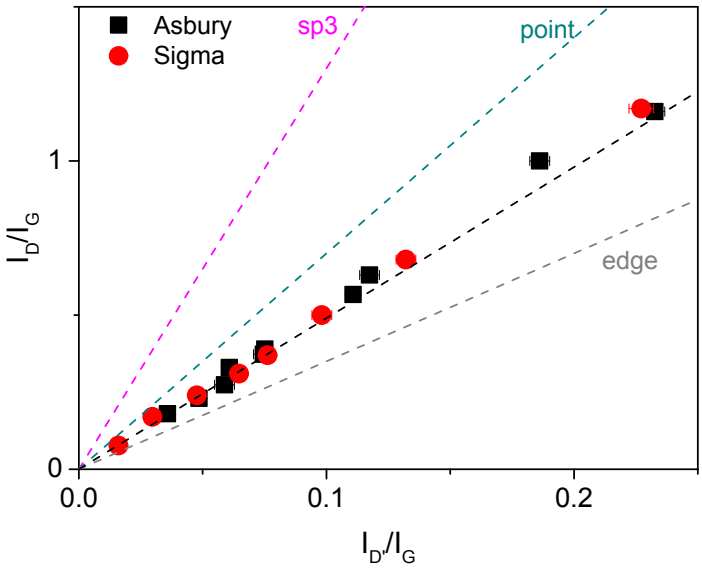

Figure S25: Plot of I_D/I_G ratio versus $I_{D'}/I_G$ ratio obtained from fitting the spectrum in this region to two Lorentzians. As suggested by Eckmann et al.,[8] the $I_D/I_{D'}$ intensity ratio can serve as an indicator for the defect type as indicated by the dashed lines in the figure. In the case of our samples, the $I_D/I_{D'}$ is between values expected for point and edge defects suggesting that the parent graphite is not defect free.

3.5 Alternative metrics for N

As stated in the main text, we have looked at several alternative approaches to describe the changes in the 2D-band shape, position and intensity. First, we have attempted to use the intensity of the 2D-band at a single fixed wavenumber, normalized to the G-band intensity. Normalising this ratio to the value measured for the parent graphite (in analogy to M_2, see main text) yields the value M_3, plotted in Figure S26.

$$M_3 = \frac{\left[I_{2690}/I_G\right]_{G'ene}}{\left[I_{2690}/I_G\right]_{G'ite}} \tag{S13}$$

The number of layers can then be obtained according to equation S14

$$< N >= 21.5 \cdot M_3^{-1.96} \tag{S14}$$

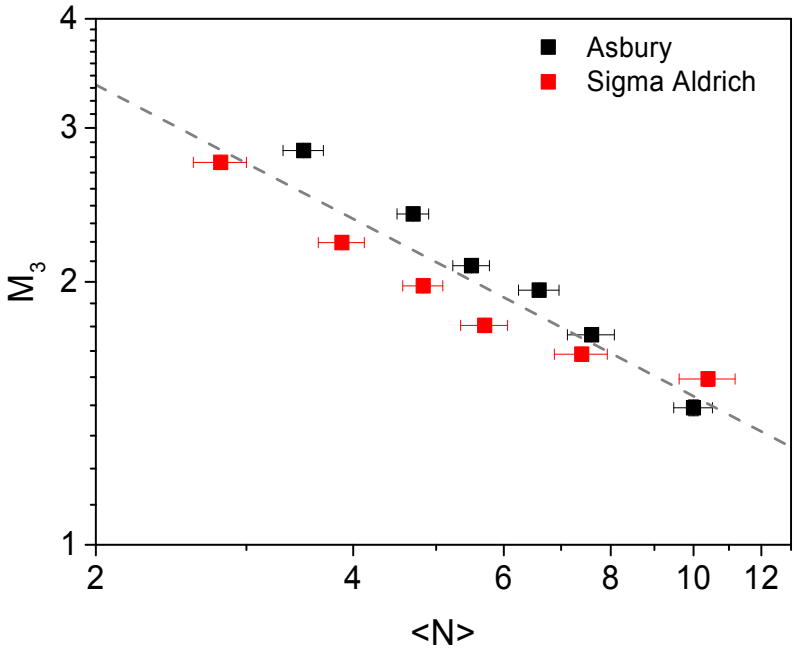

Figure S26: Value of metric M_3 for nanosheet thickness based on the normalized intensity of the 2D-band at 2690 cm^{-1}, normalized to the value from the parent graphite. Line shows fit to equation S14.

However, while this produced a usable metric, it has the drawback that the spectrum of the parent graphite is required. For end-users of graphene, this will not always be available or

measurable. We have therefore attempted to plot the metric without normalizing to the parent graphite value, giving

$$M_4 = \left[I_{2690cm^{-1}} / I_G \right]_{G'ene} \quad \text{(S15)}$$

This is plotted in Figure S27, showing that this still gives a usable metric for average layer number through equation S16.

$$< N >= 1.2 \cdot M_4^{-2} \quad \text{(S16)}$$

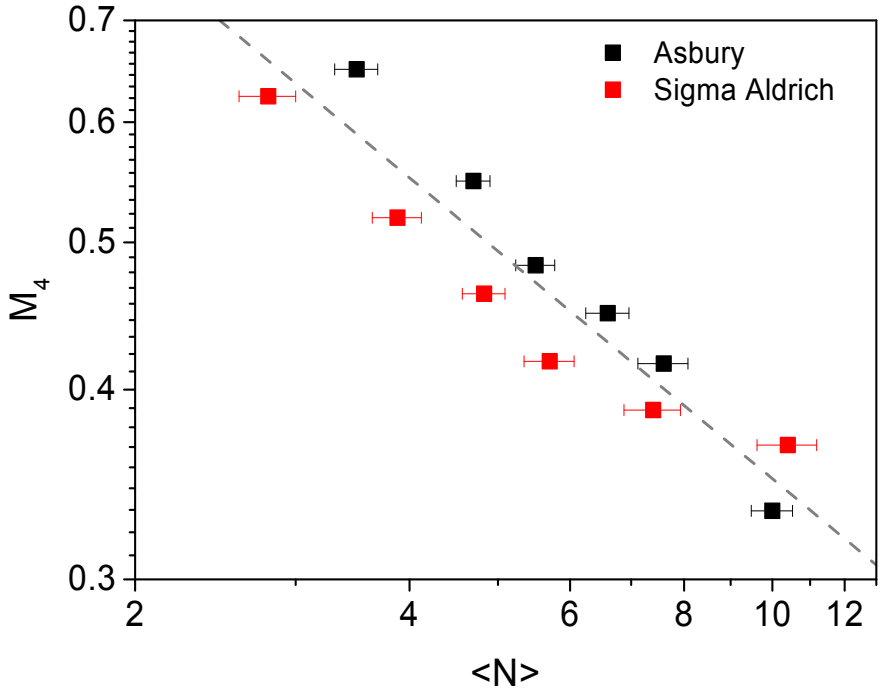

Figure S27: Value of alternative metric for average layer number based on normalized intensity of the 2D-band at a fixed wavenumber. In this case, M_4 uses the intensity at 2690 cm^{-1}. Line shows fit to equation S16.

While both of these alternative values could be used for a metric for <*N*> they both have the problem that they use the intensity at a fixed wavenumber. The result of this is that the value becomes sensitive to any instrumental shifts in the position of the spectra. While these can be corrected after measurement by manually shifting the spectra, we would prefer a metric that does not require such adjustments, as peak shifts can also potentially be a result of strong

doping. For this reason, we propose the use of the maximum value of the 2D-band, as described in the main text (M_1) even though it may be limited to standard solvent and surfactant systems.

It has been proposed that an alternative approach to avoid this issue is to use the FWHM of the 2D-band (Γ_{2D}).[9, 10] We have found that this offers a reasonable metric for our graphene dispersions only for smallest fractions, up to $< N > \approx 8$ for Asbury samples, and $< N > \approx 5$ for Sigma Aldrich samples. As shown in Figure S28, within this range, the behaviour is well defined, and matches with the value for turbostratic graphite[11, 12] even though the 2D-band widths are larger compared to measurements of individual nanosheets such as monolayer graphene with a 2D-band width of ~20-25 cm^{-1}.The number of layers can be calculated according to equation (S17).

$$< N >= \frac{\Gamma_{2D} - 50.3}{3.05} \qquad \text{(S17)}$$

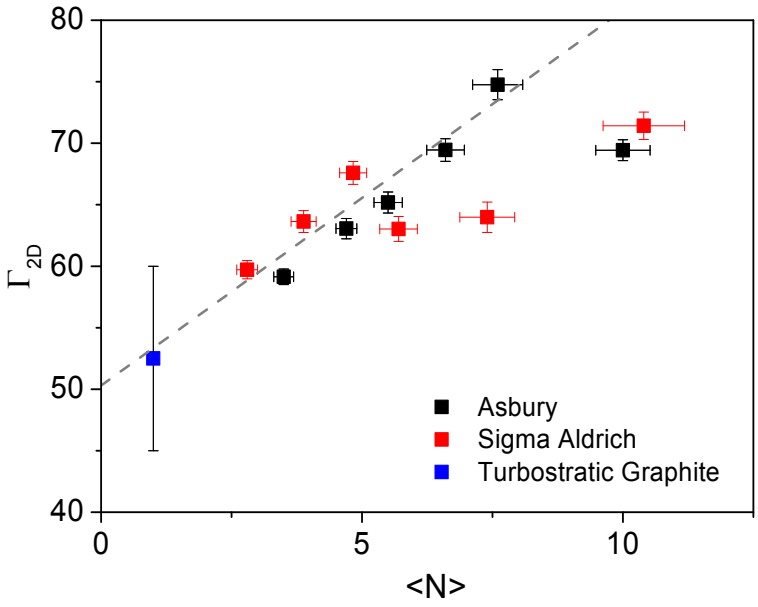

Figure S28: Width of 2D-band, obtained by fitting the band to a single Lorentzian peak. Also shown is the literature value of turbostratic graphite. The line shows the fit to equation S17.

Damm *et al.*[10] have suggeted that the presence of defects and edges can also lead to broadening of the 2D-band, separate to the effect of the layer number. We have attempted to account for this contribution by normalizing the Γ_{2D} value by the I_D / I_G ratio (without subtracting the I_D / I_G ratio of the parent graphite) and taking the inverse, such that

$$M_5 = \frac{I_D/I_G}{\Gamma_{2D}} \tag{S18}$$

Figure S29 shows this offers a further metric to obtain the average number of monolayers per nanosheet for both graphite sources, and across the full range thicknesses. However, it has limitations when the graphene sheets are large. Simply because no D-band would be present and hence this metric would yield a value of zero, regardless of the number of layers. Despite this, we can propose a metric based on this measure according to equation S19.

$$< N >= 4.67 \cdot M_5^{-1.65} \tag{S19}$$

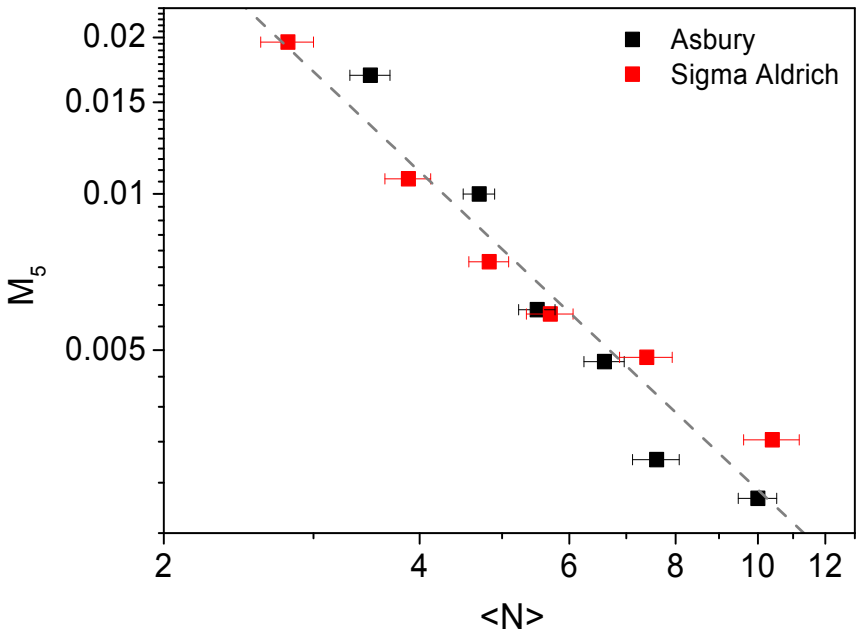

Figure S29: Value of alternative metric, M_5 as a function of average number of monolayers per nanosheet. Line shows a fit to equation S19.

Note that the values of 2D-band width have been found by fitting the 2D-band to a single Lorentzian peak, even for the largest fractions, where this results in a very poor fit (see Figure S30). For the samples produced from Asbury graphite, we have also manually measured FWHM from the spectra. While for the values for the width itself show significant differences, there were no significant differences in the value of M_5 (Figure S31).

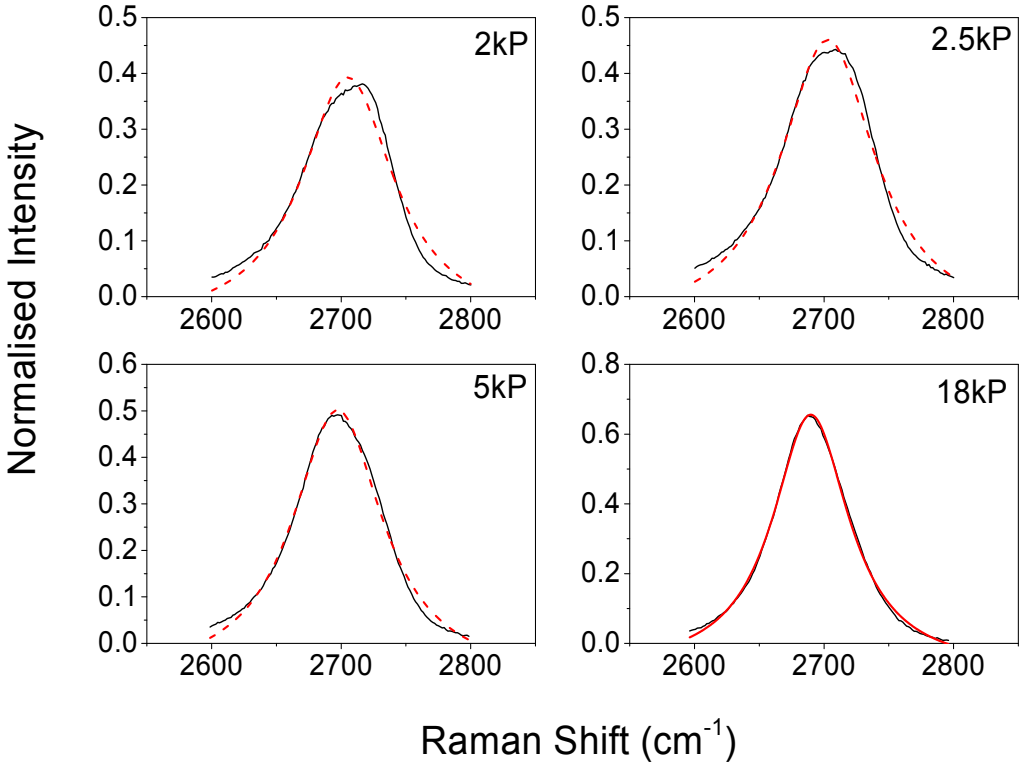

Figure S30: Examples of fitting of 2D-band to a single Lorentzian peak to obtain a value for the peak width. It can be seen that while for thin nanosheets, (e.g. 18kP) this yields a reasonable fit, for samples with thick nanosheets, the fit becomes increasingly poor.

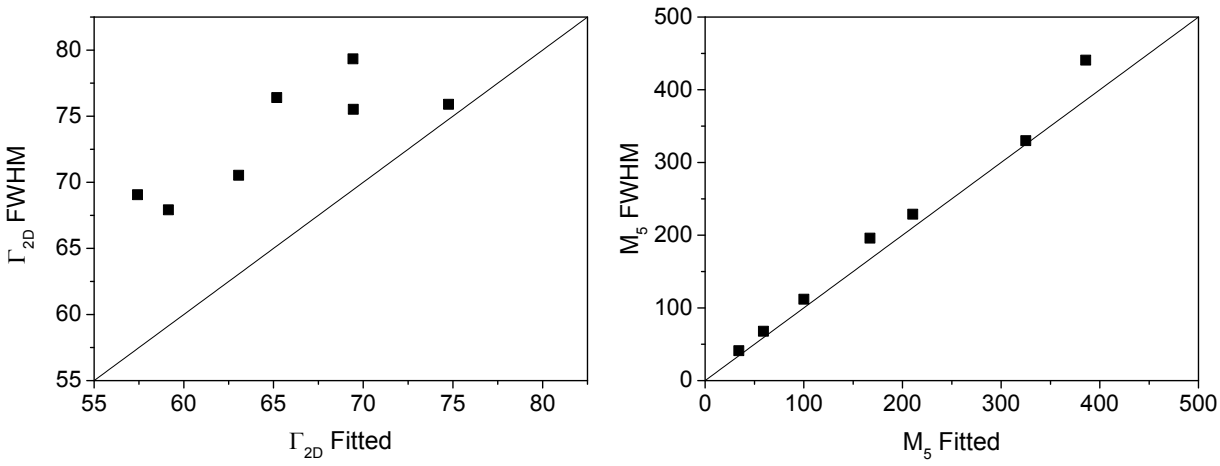

Figure S31: Comparison of methods to obtain width of the 2D band. While values obtained by reading the FWHM directly from the spectra gives higher values than from fitting a single Lorentzian (left), there are no significant differences in the resulting values of M_5 (right).

3.6 Impact of averaging

Due to spatial variation across the filtered graphene films, the values presented in this work have been the average of 100-120 spectra over an area 20 μm x 20 μm (see *Methods*). These spectra are then averaged, and the resulting spectra corrected for the baseline, then normalized to the G-peak intensity. In order to estimate the uncertainty in the intensity values we obtain, we have taken a subset of 20 spectra and processed the raw spectra in three ways. Firstly, we normalized these to the G-peak inensity individually (without baseline correction), then averaged, then baseline-corrected and the standard deviation of the intensity at various positions recorded. Secondly, we have baseline-corrected the individual spectra first, and then normalized and averaged the spectra. Finally, the spectra have been averaged before baseline correction and normalization (the standard process). The results of this analysis are shown in Table S1 showing that there is little difference in the values of the intensity at any of the significant positions, with the standard deviation in all cases being 0.03 or less. We have therefore use a value of 0.03 for error bars in all intensity ratios presented here.

Table S1: Analysis of uncertainty in Raman intensity values arising from averaging of spectra.

	I_D	$\sigma(I_D)$	I_{2690}	$\sigma(I_{2690})$	I_{2690}	$\sigma(I_{2720})$
Normalized, Averaged	0.37	0.02	0.416	0.022	0.380	0.017
Corrected, Normalized, Averaged	0.37	0.03	0.403	0.025	0.369	0.022
Averaged, Corrected, Normalized	0.37	0.028	0.402	0.02	0.366	0.020

While there is no effect seen in the intensity ratios, it is reasonable to expect that there may be a greater effect on the width of peaks, especially as there may be slight spectral shifts between locations. We have therefore analyzed the width of the G-band from 20 individual spectra, and compared this to the value for the averaged spectrum. Figure S32 shows a histogram of the width measured from the individual spectra, giving a mean of 24.2 cm^{-1} and a standard deviation of 0.7 cm^{-1}. This compares to a value of 24.18 cm^{-1} from the averaged

spectrum, confirming that there is no effect on the peak widths as a result of averaging several spectra.

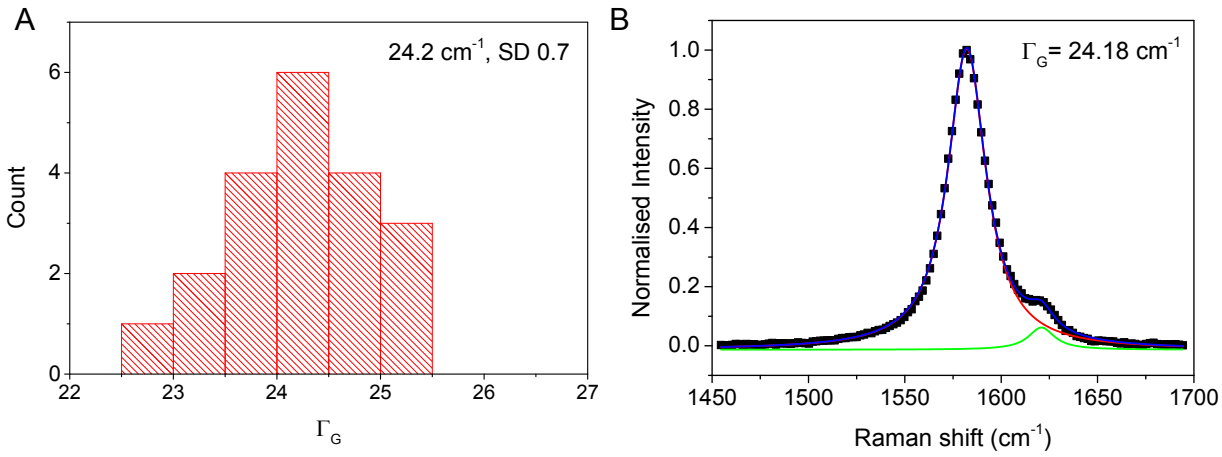

Figure S32: A) Histogram of G-peak widths showing a mean value of 24.2 cm^{-1}. This matches the value of 24.18 cm^{-1} obtained from the averaged spectrum (B).

4 Number mean *versus* volume fraction mean

Throughout the main manuscript, the spectroscopic metrics were related to the arithmetic number average (or number mean) of the population of the nanosheets. However, spectroscopy probes the volume/mass rather than the number. Hence, technically, it would be necessary to weight the number mean values with the volume fractions (Vf). As we will show below, this is not required, as mean values which are weighted with volume fractions are correlated to the number mean values in a well defined way. Therefore, the mean of the number population can be extracted from spectroscopy.

To weight the mean values for nanosheet length and thickness, it is required to determine the volume fractions of the individual nanosheets in a given sample. Volume fractions can be estimated from statistical AFM, as long as nanosheet thickness and size (length and width to estimate the area) are recorded simulatneously. However, there are a few problems associated with this process, and so we have analyzed values of the number average throughout the main manuscript. The first problem is that an error is associated with the determination of nanosheet size (length) from AFM. In particular the size of smaller nanosheets is overestimated due to tip broadening and pixilation effects (see figure 1D). Hence, mean nanosheet length (and, to a greater extent, volume fraction weighted length) will not be accurate. In turn, number average values can be easily determined from TEM (as used throughout the main manuscript). However, with TEM, determination of volume fractions is extremely challenging as each nanosheet would need to be imaged in low resolution and multiple times at high resolution to inspect edges (to count layer number). Secondly, the analysis becomes much more time consuming. For example, the number of data points required to determine reliable mean values depends on the width of the distribution. In the case of the size-selected samples, we have realized that number mean values do not change significantly when > 70 (in the case of small and thin) to >100 (in the case of larger, thicker) nanosheets are counted. However, this is not the case for an accurate determination of volume fractions, where we estimate that 250-300 counts are required. In addition, the layer number of nanosheets protruding from a reaggregated ensemble can still be analyzed (allowing for determination of number mean N), but no information on lateral size can be extracted. Therefore, significantly more images would be required to obtain statistically relevant data. Given the large number of samples that were analyzed to establish robust metrics, volume fraction weighting would not have been feasible.

However, due to the importance of this point, we have attempted to carry out such an analysis on one data set (Asbury graphite including stock). First, we plot the volume fraction weighted mean thickness and length *versus* the respective number mean in figure S33. In both cases, we find a well-defined correlation that can be fit with an exponential (dashed line) with the data points of the stock dispersion collapsing on the same curve. We note that the data is significantly more scattered in the case of nanosheet length compared to thickness because length distributions are typically broader (see above). Nonetheless, this relationship implies that the spectroscopic data can be correlated to number mean values.

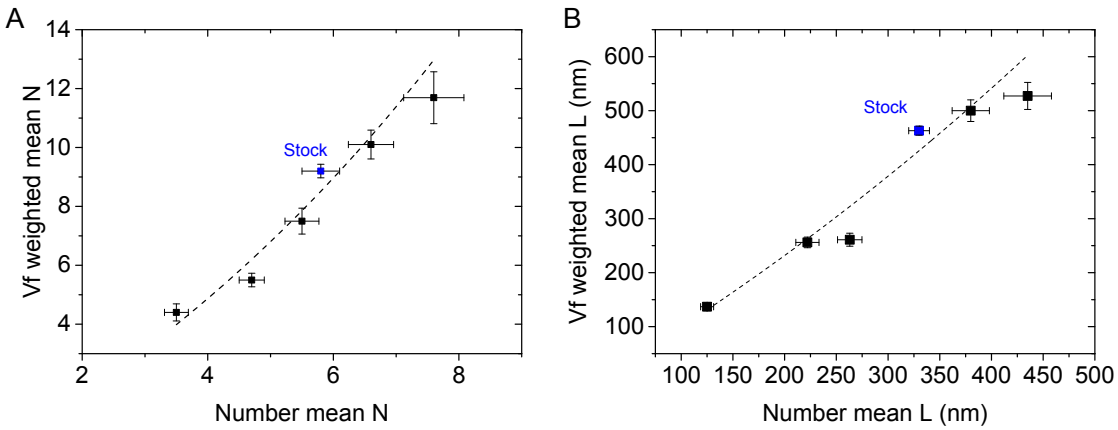

Figure S33: Mean values weighted with volume fraction plotted versus number mean values (Asbury graphite). A) Number of layers, B) Nanosheet length.

In figures S34-35 we plot the metric values established in the main manuscript for number means as well as volume fraction weighted means. Since volume fraction weighted mean values are larger than number mean values (see figure S33), a different quantitative relation is obtained. However, it is very clear that the same trends are discernible, in particular in the case of the thickness metrics from UV-vis (figure S33) and Raman (figure S35A and B) spectroscopy. Unfortunately, the data for the length metrics (figure S35C and D) with L being determined from AFM (black data points) is extremely scattered and does not even collapse on the number mean fit curve shown in the main manuscript which was established based on the TEM analysis. A similar picture is obtained from the volume weighted mean length (red data points in figure S35C and D).

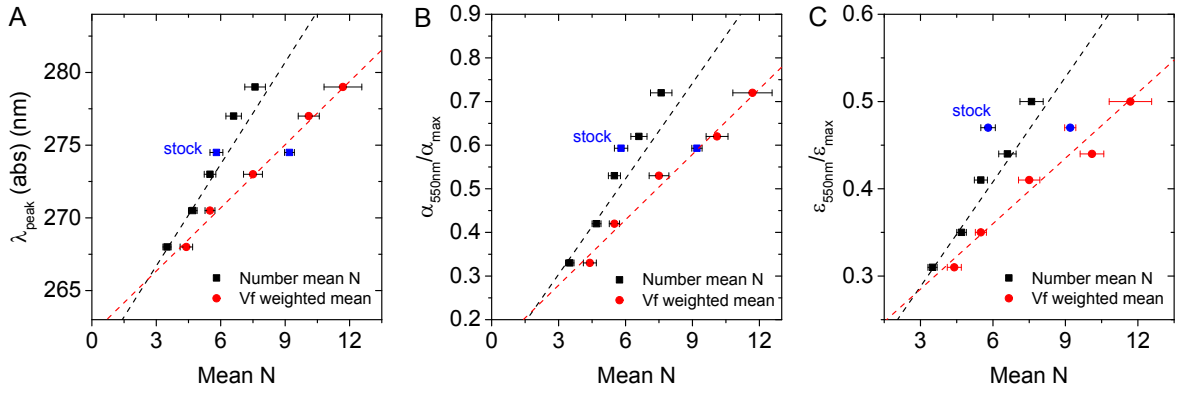

Figure S34: UV Vis mean N metrics plotted against both number mean (same data as in main manuscript) and volume fraction weighted mean (Asbury graphite data). Weighting by volume fractions gives a different quantitative relationship between the metric values and the mean thickness due to the underlying relationship in figure S31. However, the same trends are apparent. The black dashed lines are the fits from the main manuscript. The red-dashed line represent the quantitative relationship between metric value and volume fraction weighted mean. A) Absorbance peak position, B) absorbance intensity ratio Abs_{550}/Abs_{max}, C) extinction intensity ratio Ext_{550}/Ext_{max}.

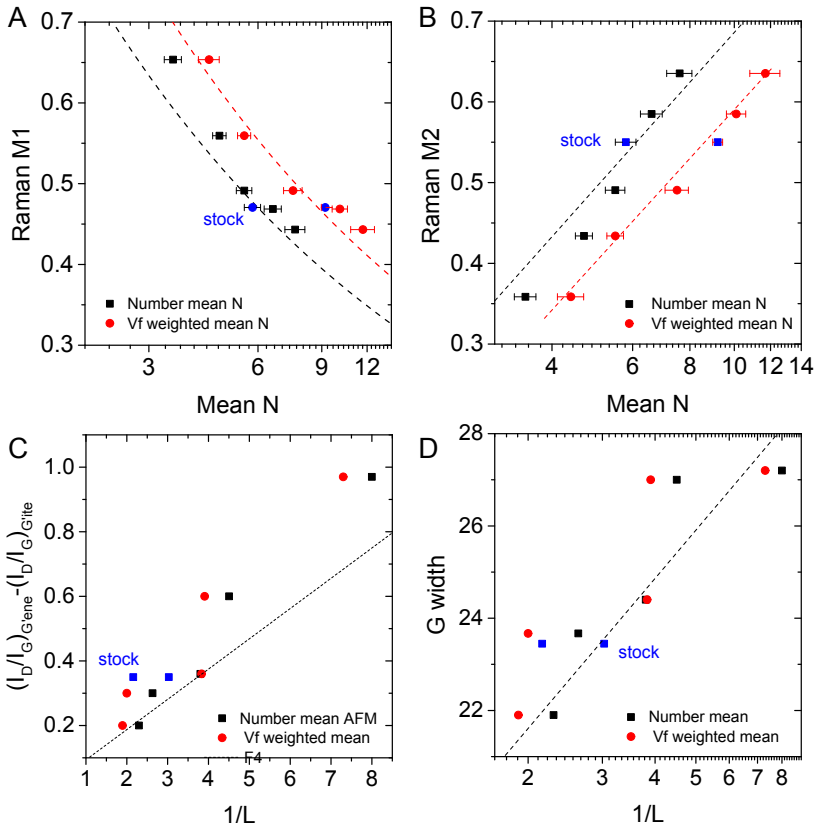

Figure S35: Raman metrics plotted against both number mean (same data as in main manuscript) and volume fraction weighted mean (Asbury graphite data). Similar to the UV Vis metrics (figure S32), a different quantitative, but similar qualitative behavior is observed. The black dashed lines are the fits from the main manuscript. The red-dashed line represent the quantitative relationship between metric value and volume fraction weighted mean. A) Raman M1 metric for thickness (intensity ratio of 2D/G band), B) Raman M2 metric for thickness (see main manuscript. C) D/G length metric, D) G width length metric. The scatter in the data for the lengh metrics with L determined from AFM (necessary for volume fraction weighting) is signigicant, as a precise determination of length from AFM is very challenging.

5 References

1. C. Backes, R. J. Smith, N. McEvoy, N. C. Berner, D. McCloskey, H. C. Nerl, A. O'Neill, P. J. King, T. Higgins, D. Hanlon, N. Scheuschner, J. Maultzsch, L. Houben, G. S. Duesberg, J. F. Donegan, V. Nicolosi and J. N. Coleman, *Nature Communications*, 2014, **5**, 4576.
2. K. R. Paton, E. Varrla, C. Backes, R. J. Smith, U. Khan, A. O'Neill, C. Boland, M. Lotya, O. M. Istrate, P. King, T. Higgins, S. Barwich, P. May, P. Puczkarski, I. Ahmed, M. Moebius, H. Pettersson, E. Long, J. Coelho, S. E. O'Brien, E. K. McGuire, B. M. Sanchez, G. S. Duesberg, N. McEvoy, T. J. Pennycook, C. Downing, A. Crossley, V. Nicolosi and J. N. Coleman, *Nature Materials*, 2014, **13**, 624-630.
3. D. Hanlon, C. Backes, E. Doherty, C. S. Cucinotta, N. C. Berner, C. Boland, K. Lee, P. Lynch, Z. Gholamvand, A. Harvey, S. Zhang, K. Wang, G. Moynihan, A. Pokle, Q. M. Ramasse, N. McEvoy, W. J. Blau, J. Wang, G. Abellan, F. Hauke, A. Hirsch, S. Sanvito, D. D. O'Regan, G. S. Duesberg, V. Nicolosi and J. N. Coleman, *Nature Communications*, 2015, **6**, 8563.
4. A. Harvey, C. Backes, Z. Gholamvand, D. Hanlon, D. McAteer, H. C. Nerl, E. McGuire, A. Seral-Ascaso, Q. M. Ramasse, N. McEvoy, S. Winters, N. C. Berner, D. McCloskey, J. Donegan, G. Duesberg, V. Nicolosi and J. N. Coleman, *Chemistry of Materials*, 2015, **27**, 3483–3493.
5. G. S. He, H.-Y. Qin and Q. Zheng, *Journal of Applied Physics*, 2009, **105**, 023110.
6. M. Lotya, Y. Hernandez, P. J. King, R. J. Smith, V. Nicolosi, L. S. Karlsson, F. M. Blighe, S. De, Z. Wang, I. T. McGovern, G. S. Duesberg and J. N. Coleman, *Journal of the American Chemical Society*, 2009, **131**, 3611-3620.
7. M. Lotya, P. J. King, U. Khan, S. De and J. N. Coleman, *ACS Nano*, 2010, **4**, 3155-3162.
8. A. Eckmann, A. Felten, A. Mishchenko, L. Britnell, R. Krupke, K. S. Novoselov and C. Casiraghi, *Nano Letters*, 2012, **12**, 3925-3930.
9. D. S. Lee, C. Riedl, B. Krauss, K. von Klitzing, U. Starke and J. H. Smet, *Nano Letters*, 2008, **8**, 4320-4325.
10. C. Damm, T. J. Nacken and W. Peukert, *Carbon*, 2015, **81**, 284-294.
11. L. M. Malard, M. A. Pimenta, G. Dresselhaus and M. S. Dresselhaus, *Physics Reports*, 2009, **473**, 51-87.
12. L. G. Cançado, K. Takai, T. Enoki, M. Endo, Y. A. Kim, H. Mizusaki, N. L. Speziali, A. Jorio and M. A. Pimenta, *Carbon*, 2008, **46**, 272-275.